2015

Droplet actuator system for molecular diagnostic applications

Riley Brien
Iowa State University

Droplet actuator system for molecular diagnostic applications

by

Riley Brien

A thesis submitted to the graduate faculty

in partial fulfillment of the requirements for the degree of

MASTER OF SCIENCE

Major: Electrical Engineering

Program of Study Committee:
Santosh Pandey, Major Professor
Meng Lu
George Amariucai

Iowa State University

Ames, Iowa

2015

TABLE OF CONTENTS

Page

LIST OF FIGURES

Page

LIST OF TABLES

Page

ACKNOWLEDGMENTS

I would like to thank my major professor, Dr. Santosh Pandey, who guided and supported me in my research. My skills as a researcher expanded rapidly under his guidance, from writing manuscripts to designing experiments. I could not have asked for a more helpful and competent advisor. I appreciate the support of my committee members, Dr. Meng Lu and Dr. George Amariucai, who provided helpful feedback on my thesis. This thesis was funded by a National Science Foundation Graduate Research Fellowship (GRFP) (Grant Number DGE1247194).

My graduate studies would not have been so successful without the help and support of my colleagues, family, and friends. From my lab group, Taejoon Kong deserves much credit for assisting me in performing experiments as well as discussing new research ideas. I would also like to thank my labmate Zach Njus for his guidance and expertise in developing software for research.

I appreciate the help of my family, who have always supported and encouraged me to pursue my goals. My mother and father, Gail and Michael Brien, gave me the opportunity to succeed and devoted their efforts to helping me at each stage. My older sister Kaitlin was always an excellent role model and a motivator to achieve academic success. I hope to have a similar influence on my younger brother, Nicholas, who I always enjoy spending time with to relax.

ABSTRACT

In biological research, routine liquid handling operations require considerable human effort and manual labor. For this reason, experiments in clinical laboratories are time-consuming and thus expensive. Recently, advances in point-of-care "lab-on-a-chip" systems have allowed more efficient ways of sample handling and analysis. Such systems often operate by automated manipulation of discrete liquid droplets, and are increasing sought to improve experimental throughput. Various techniques have been developed to manipulate discrete droplets, such as digital microfluidics, surface acoustic waves, and texture ratchets. In this thesis, a novel droplet actuation system is presented that can be applied for molecular diagnostic tests. The system utilizes a motor-driven platform to manipulate droplets on a superhydrophobic surface patterned with hydrophilic symbols. The design of the system components and the various fluid-handling operations are presented, such as merging, mixing, dispensing, and splitting. A colorimetric glucose concentration assay is realized on the presented platform to measure levels of glucose in sheep serum samples. Our colorimetric experiments match favorably with the gold standard spectrophotometric method. These results indicate that the droplet actuator is a promising system for automating fluid-handling steps in biological experiments.

CHAPTER 1
INTRODUCTION TO DROPLET ACTUATION TECHNIQUES

1.1 Background and Motivation for Droplet Actuation

Performing biological research requires handling small volumes of liquid, which is typically done by manual micro-pipetting.[1] Experiments generally require multiple pipetting manipulations of liquid samples and reagents, which are performed in vials, test tubes, or microwell plates. Automating these pipetting steps offers increased efficiency and fewer opportunities for technician error. For this reason, several commercially available liquid handling robots have been developed that contain multi-channel robotic pipetting arms. These liquid handling robots are large and expensive, however, limiting their use to laboratories requiring high-throughput sample processing.

An alternative method of liquid handling called digital microfluidics was invented 15 years ago, which can be less expensive and more compact than a liquid handling robot.[2] This technique allows discrete droplets to be actuated (transported) across an electrode array using the electrowetting effect. As discussed in the next sections, digital microfluidics and several other droplet actuation techniques have gained attention for providing automated liquid handling for biological applications. These techniques inspired our new method of droplet actuation described in Chapter 2, which has proven capable of performing biological experiments in Chapter 3.

1.2 Digital Microfluidics

1.2.1 Applications and Principles of Digital Microfluidics

Digital microfluidics has facilitated research in biology by enabling precise, automated control of discrete droplets. Several digital microfluidic systems have been implemented for a variety of biological applications. For example, digital microfluidic chips capable of manipulating and thermal cycling discrete droplets were used for DNA amplification of Dengue II virus cDNA in a real-time polymerase chain reaction device.[3] Mammalian cell culture chips using droplets to perform cell seeding, media exchange, and cell detachment have also been demonstrated.[4] Other examples include

immunoassays to detect rabbit IgG antigens and enzymatic assays to detect glucose concentrations in human physiological fluids.[5,6] Digital microfluidics also offers applications in diagnostic screening, as one group has developed a platform for screening for lysosomal storage diseases in newborns using the technology.[7, 8]

Digital microfluidic devices can actuate droplets on an array of insulated electrodes by applying high electric potentials. This can be accomplished by sandwiching droplets between a bottom electrode array and a top ground plate.[8] Figure 1.1 shows the configuration of such a device.[9] As a high electric potential is applied to a neighboring electrode, the droplet experiences electrostatic forces that cause it to move to the "active" electrode. The electrodes must be insulated from the droplets by a thin dielectric layer with a material such as Parylene, and a hydrophobic layer such as Teflon can be used to reduce droplet adhesion. Actuation voltages can be on the order of 150-250 volts.

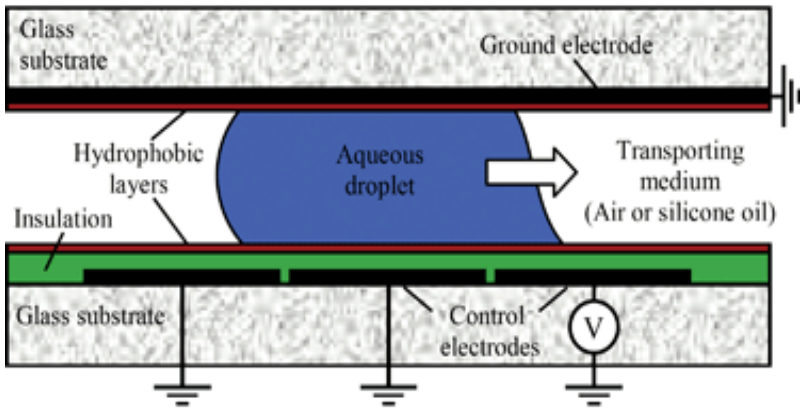

Figure 1.1. Digital microfluidics electrode array configuration.[9]

Sequential actuation of multiple electrodes can produce droplet transport, which is a key liquid handling operation. Figure 1.2 shows other operations that can be performed on a digital microfluidic electrode array.[10] Two or more droplets can be merged together onto the same electrode, and then mixed by transporting back and forth across the surface. Splitting a droplet is possible by actuating two neighboring electrodes simultaneously, causing the droplet to stretch in opposite directions. Dispensing can be achieved by creating larger reservoir electrodes adjacent to smaller electrodes, then performing an asymmetrical splitting operation. With these basic operations, researchers

and companies have been able to apply digital microfluidics to applications where automated handling of small volumes of liquid is desirable.

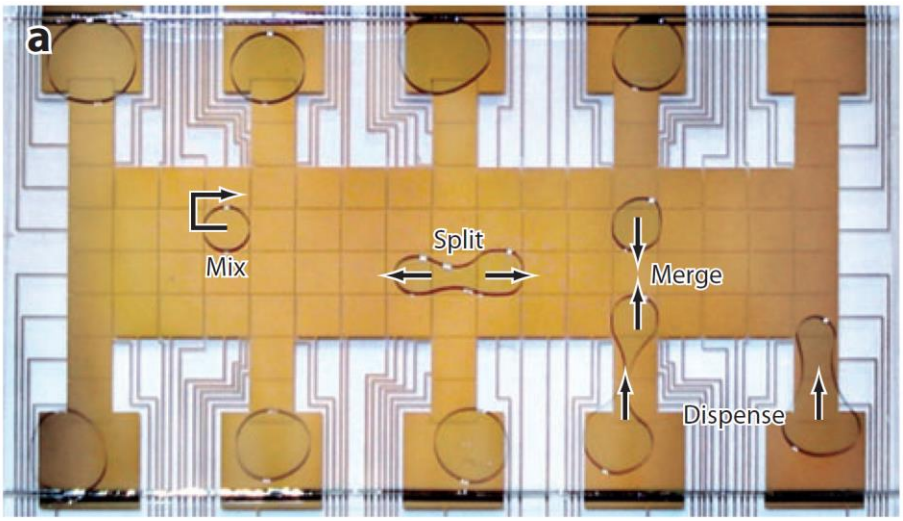

Figure 1.2. Digital microfluidic droplet operations.[10]

To illustrate one example of how digital microfluidics can be used for biological applications, Figure 1.3 shows the configuration of a digital microfluidic system for performing estrogen assays in breast tissue, blood, and serum. Estrogen concentration is a relevant measurement for identifying women at risk of developing breast cancer.[11] Conventionally, measuring estrogen concentrations requires biopsy of large tissue samples and manual micro-pipetting to carry out the extraction procedure. The digital microfluidic device, however, requires smaller breast tissue samples, and the processing is done without manual intervention. The sample and reagent are loaded into the device, and the following droplet manipulation steps are performed: The lysing agent is merged and mixed with the blood sample; Next, the polar and nonpolar extractions are completed; Finally, the sample is collected and analyzed via mass spectrometry.

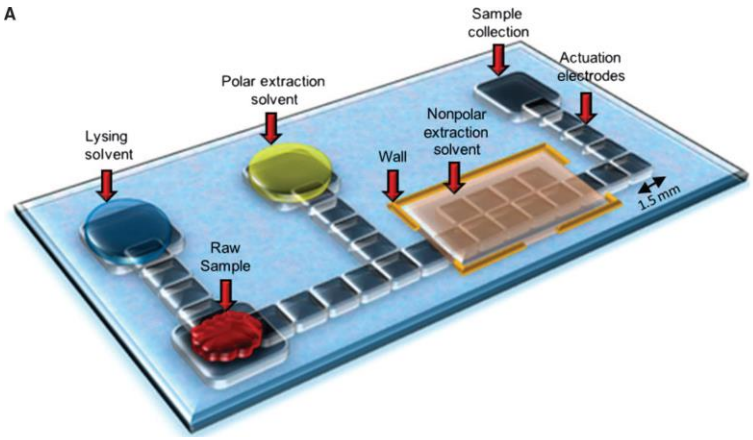

Figure 1.3. Digital microfluidic system for estrogen assay.[11]

1.2.2 Prototype Digital Microfluidic System

A prototype digital microfluidic system was constructed by our group in order to explore its capabilities for droplet manipulation. Figure 1.4 shows the components of the system, including the high voltage control system and the electrode array upon which the droplets are actuated. The system was able to transport, merge, and mix two droplets, as shown in Figure 1.5.

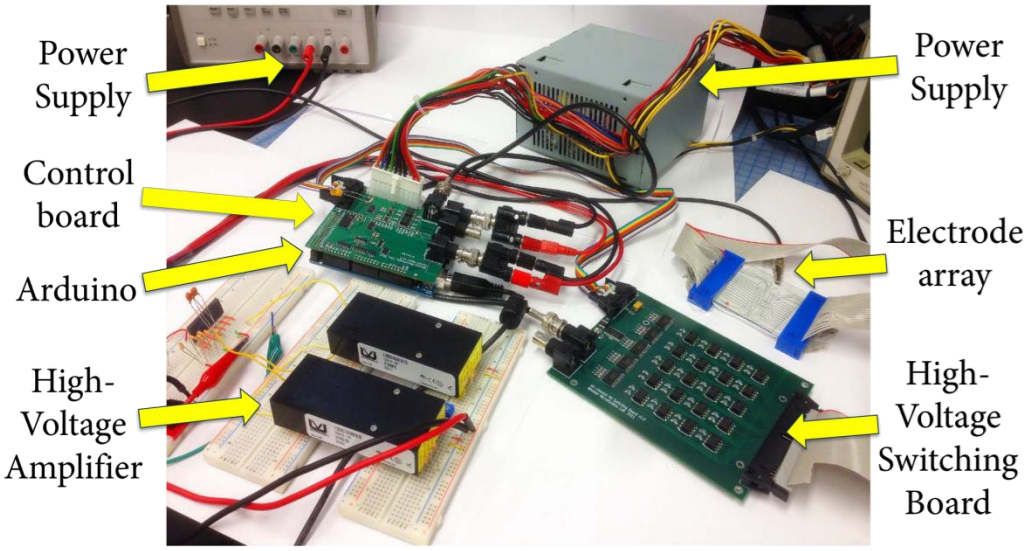

Figure 1.4. Our digital microfluidic prototype system.

Although key droplet operations could be performed, challenges were faced when constructing the system. First, fabricating electrode arrays without cleanroom facilities produced low yields and devices with many inoperable electrodes. Coating the insulating Parylene C layer required sending the electrode arrays to an external company with the appropriate chemical vapor deposition equipment. After the lengthy fabrication procedure, electrode arrays were prone to failure when large actuation voltages were applied. Consequently, other methods of droplet manipulation were investigated.

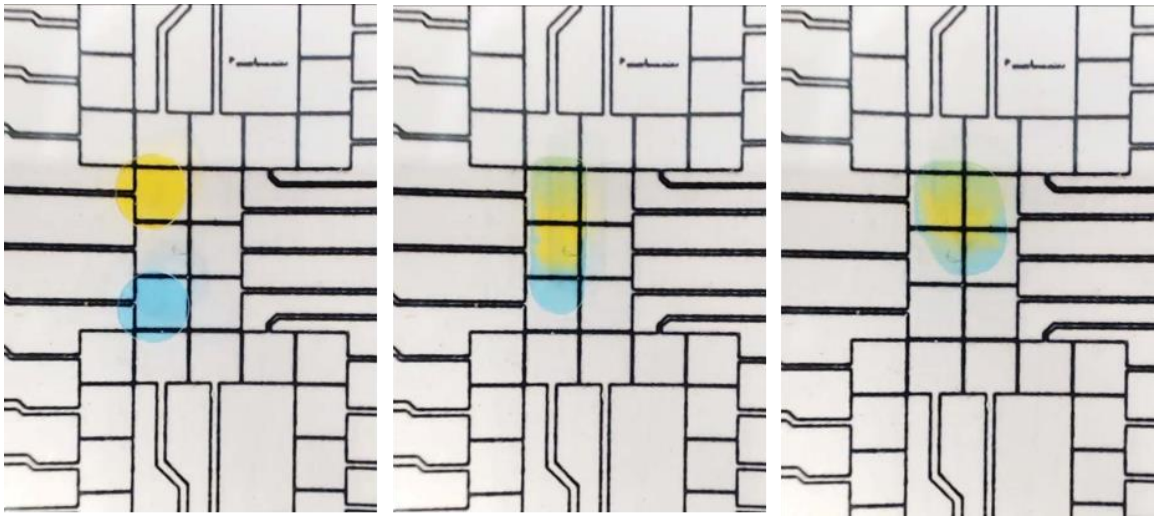

Figure 1.5. Our digital microfluidic electrode array demonstrating merging and mixing operations.

1.3 Open-Surface Droplet Actuation

1.3.1 Open-Surface Droplet Actuation Techniques

Recently, open-surface microfluidics has gained increased attention, due in part to greater accessibility. In addition, these devices provide a clear optical path, no cavitation or obstruction, and device reusability.[12] However, manipulating droplets on these open-surface devices using the digital microfluidics technique requires higher voltages. Instead, other techniques have been developed to manipulate droplets on open surfaces. For instance, optoelectrowetting utilizes photoconductive materials and a light beam to activate an array of electrodes similar to digital microfluidics.[13] Surface acoustic waves are also capable of manipulating droplets, and one group has implemented a polymerase

chain reaction device using this technique.[14] A similar polymerase chain reaction device was demonstrated using magnetic beads to actuate each droplet.[15,16] In addition, texture ratchets can drive droplet transport through acoustic vibrations.[17]

Figure 1.6 shows the design and operation of a texture ratchet device that consists of a silicon substrate patterned with micro-scale "rungs" and "pillars." Upon vibration, the leading edge of the droplet experiences increased wetting relative to the trailing edge, which causes the droplet to be transported along the texture ratchet. Fabricating intersecting texture ratchets makes it possible to merge and mix two droplets. Splitting and dispensing have not been demonstrated using texture ratchets.

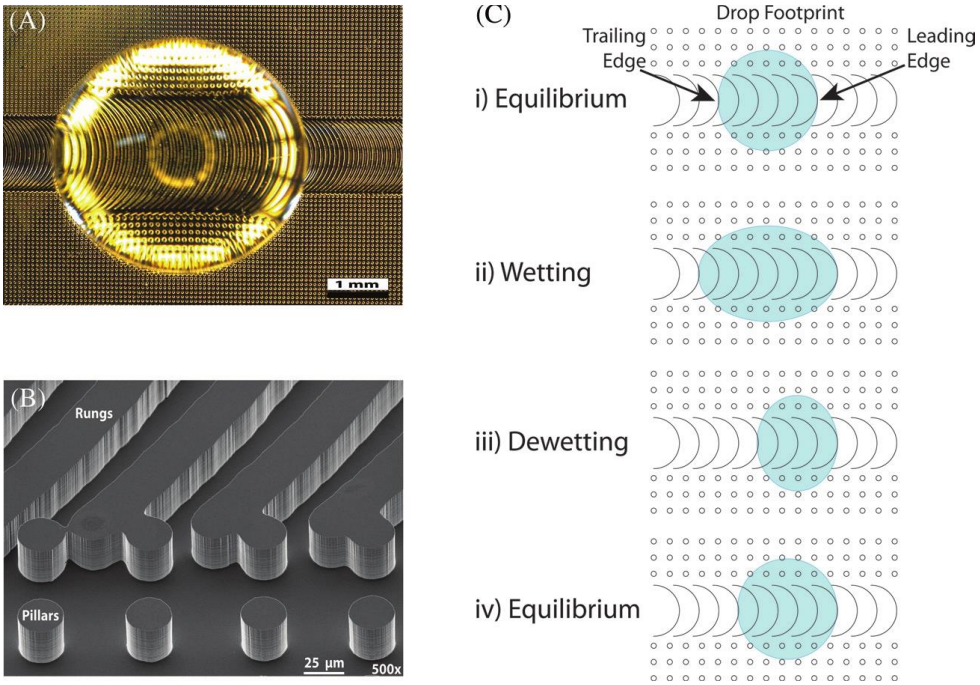

Figure 1.6. Texture ratchet design and operation.[17]

1.3.2 Comparison of Active Droplet Manipulation Techniques

The benefits of the above mentioned methods in manipulating droplets are well recognized, but disadvantages of these techniques are worth mentioning. These methods typically rely on large, complicated control systems to manipulate each droplet. Optoelectrowetting requires high light intensity, and magnetic actuation relies on expensive magnetic beads contained in each droplet. Surface acoustic wave and texture ratchet based devices can be realized only with precise fabrication techniques using

piezoelectric materials or silicon. Although surface acoustic wave devices work well in principle, scaling up to manipulate multiple droplets is challenging. For parallel processing, digital microfluidics remains the most versatile tool.

1.3 Surface Tension Confined Microfluidics

Although digital microfluidics is an attractive platform, it requires high voltages and expensive fabrication and surface coatings. This led us to seek alternative platforms with the following requirements: 12 volt power supply, disposable substrate, automated operations, the capability of handling multiple droplets, and the capability of performing basic droplet operations. To pursue this goal, passive droplet actuation by surface-tension-confined microfluidics was investigated.[18]

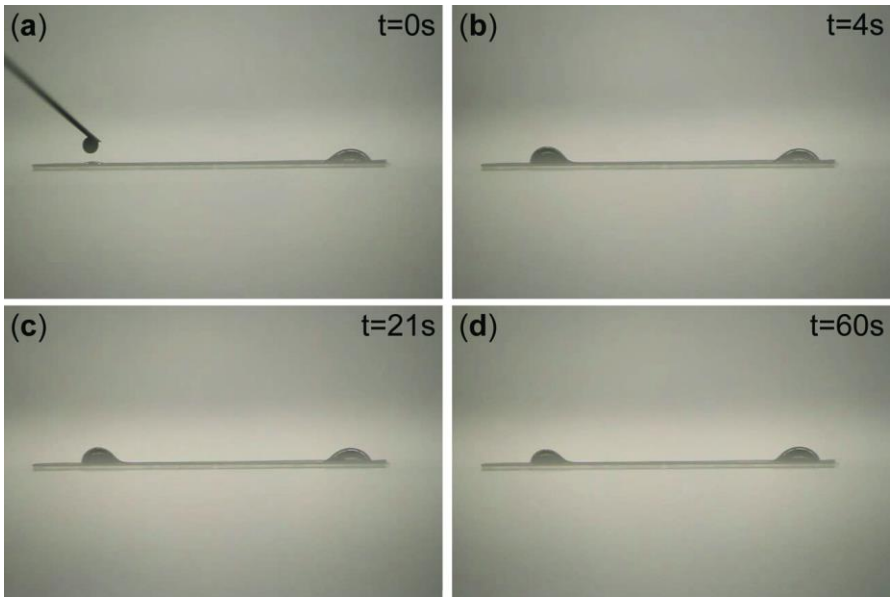

Figure 1.7. Surface tension confined microfluidic device showing the steps (**a-d**) for merging a small droplet (left) with a large droplet (right).[20]

Passive surface-tension-confined microfluidic devices control fluid flow with patterned hydrophobic and hydrophillic regions on a substrate surface. Fluid is confined to hydrophillic regions due to the contrast in wettability at the boundary with the hydrophobic region. Using superhydrophobic surfaces (contact angle greater than 150°) with roll-off angles less than 10° further facilitates fluid confinement. In recent years,

researchers have exploited various fluid transport mechanisms including chemically or spatially patterned surface wettability gradients, Laplace pressure, and gravity. One group recently demonstrated photolithographically patterned, tapered, superhydrophillic tracks on a superhydrophobic TiO_2 polymer matrix to achieve pumpless transport rates of ~150-350 μL s^{-1}.[19] Fluid was transported uphill along the tracks without providing external energy. Others have used patterned superhydrophobic surfaces to achieve fluid transport by establishing Laplace pressure gradients in which droplets of different volumes can be merged. In another work, the roll-off angle of a superhydrophobic surface was modified by patterning hydrophillic lines of varying widths. Droplets were actuated by inclining the surface to angles between 0° to 90°. Several methods, from lithography to self-assembly, microplasma writing, and inkjet printing have been used to fabricate surface-tension-confined microfluidic devices. Elsharkawy *et al.* utilized a commercially available desktop ink-jet printer with standard pigment-based ink to pattern devices capable of modifying roll-off angles and using Laplace pressure to drive flow.[20] Figure 1.7 shows the operation of the device in which a smaller droplet is mixed with a larger droplet using Laplace pressure. Droplet sampling was also achieved by depositing circular (hydrophillic) ink spots on the superhydrophobic surface, with each spot retaining a fraction of a larger droplet that flows across the surface.

CHAPTER 2
ROTATIONAL DROPLET ACTUATOR

2.1 Introduction

From the diversity of droplet actuation techniques and applications that have been developed in recent years, it is clear that this field will continue to grow. Digital microfluidics is a proven technology that is being adopted by biotechnology companies such as Illumina. Surface-tension-confined microfluidics is also a promising area of research, with passive droplet manipulation techniques being developed using simple materials. Opportunities for improvement still exist, however, as digital microfluidics devices remain costly and difficult to fabricate, while surface-tension-confined microfluidics have limited flexibility.

Although surface-tension-confined microfluidic devices are relatively simple to fabricate and require no external power source, fluid flow is irreversible, which restricts configurability compared to digital microfluidic systems. In this work, we introduce a droplet manipulation platform that combines the advantages of digital microfluidics and surface-tension-confined microfluidics. The device consists of a two-axis tilting platform driven by stepper motors, along with a patterned superhydrophobic surface upon which droplets can be transported, merged, mixed, split, and dispensed. Initially, droplets are placed on hydrophilic spots surrounded by the superhydrophobic surface. By rapidly tilting the platform from the horizontal, the droplets can be transported from one hydrophilic spot to an adjacent spot on the surface. This discrete droplet transport between hydrophilic spots is reminiscent of transport between electrodes on a digital microfluidic device. The superhydrophobic/hydrophilic patterning steps correspond to surface-tension-confined microfluidic devices.

Key advantages of our platform include simplicity, cost, and performance: The platform is controlled by a simple Arduino microcontroller that allows a series of actuation steps to be pre-programmed. The cost to fabricate the device was less than $200, and power can be supplied by a standard 12 volt wall adapter. Rapid prototyping is also possible, as fabrication of the patterned superhydrophobic surface requires two steps: spray-on coating, and ink-jet printing. These steps can be performed within one day using products available in retail stores. In addition to these benefits, the device is capable of

performing all basic droplet operations required for biological experiments. To demonstrate this functionality, two colorimetric enzymatic assays were tested, as shown in Chapter 3. The first assay measured glucose concentration of standard solutions by colorimetric detection. The second assay compared the glucose concentrations of two sheep serum samples using the colorimetric glucose indicator. These assays show the potential of the device for automated liquid handling and colorimetric quantification.

2.2 Experimental

2.2.1 Droplet Actuation System Construction

The droplet actuator relies on a two-axis tilting platform to drive droplet movement on the patterned superhydrophobic surface. Figure 2.1 shows the configuration of the system, which includes three structural components: the base, the vertical support column, and the upper platform. The dimensions of the components are as follows: base (20 cm × 20 cm × 0.5 cm); vertical support (1 cm × 1 cm × 10 cm); upper platform (10.2 cm × 10.2 cm × 1.3 cm). The three dimensional structure is drawn in AutoCAD and is machined in Plexiglas. The upper platform is connected to the vertical support column through a universal joint (Stanley Inc.), which allows two-axis rotation about a central pivot. Two stepper motors and an Arduino microcontroller with a stepper motor controller are fixed to the base with aluminum mounting brackets and double-sided tape, respectively. Each edge of the upper platform is connected to a timing belt that is driven by a pulley attached each stepper motor's shaft. A piece of elastomeric rubber tubing is attached to the end of each belt and fixed to the upper platform by a stainless steel hose clamp or zip tie. The elastomeric rubber tubing ensures adequate belt tension for the pulley system.

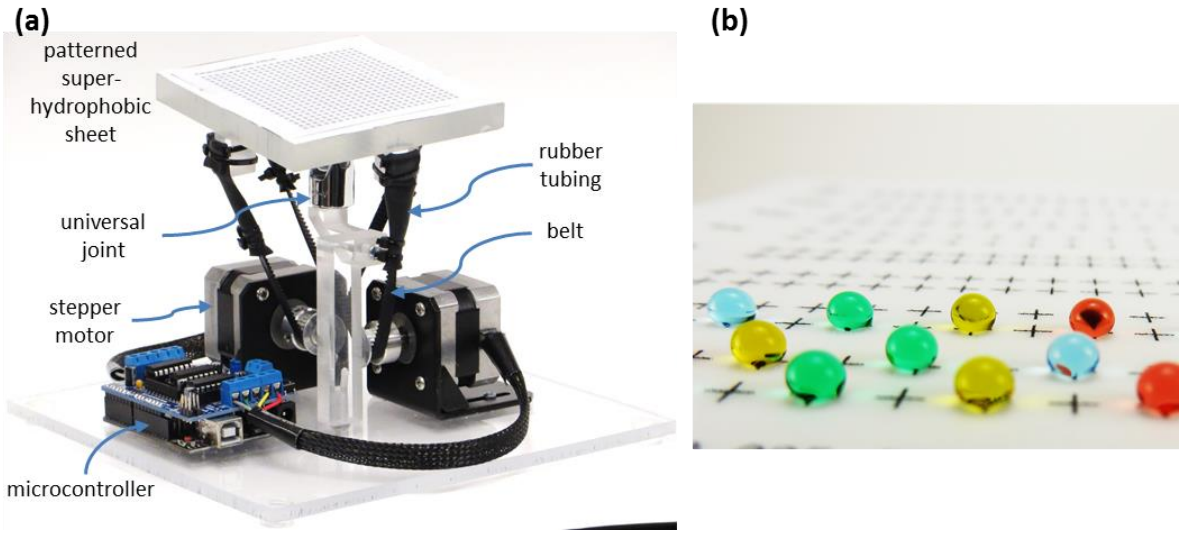

Figure 2.1. Image of the droplet actuation system. **(a)** The system comprises three components: base, vertical column, and upper platform. The base is fixed to the column. A universal joint connects the column to the upper platform. Two stepper motors, each connected with an individual belt, control the movement of the upper platform. **(b)** A hydrophobically-coated transparency film is printed with hydrophilic patterns using an inkjet printer. Individual droplets are placed on the hydrophilic patterns, which can be actuated by controlling the movement of the substrate.

The block diagram in Figure 2.2 illustrates the connections of the communication and control system. The user can interact with the device using a computer system with input devices (keyboard, mouse, etc.) and output devices (monitor, speakers, etc.). The computer communicates with an Arduino microcontroller through a USB connection using software described in Section 2.3.4. The Arduino microcontroller communicates with the stepper motor controller, which drives the stepper motors with the appropriate voltage and current (~12V, 350mA). By default, the stepper motors remain stationary. Using the computer interface, a stepper motor can be commanded to rotate with the following three parameters: number of steps (1.8° per step), stepping speed (0-200 revolutions per minute), and step direction (forward, reverse). The belt system links the stepper motor pulley to the upper platform of the droplet actuator. As the upper platform measures 10.2 cm, and the diameter of the pulley is 1.2 cm, the effective gear reduction between the motor and the platform is 1:8.5. This means each step of the stepper motor corresponds to a 0.21° rotation of the upper platform. A camera provides feedback to the

computer about droplet position and color. Monitoring the position and color of each droplet allows automated manipulation and readout of colorimetric tests.

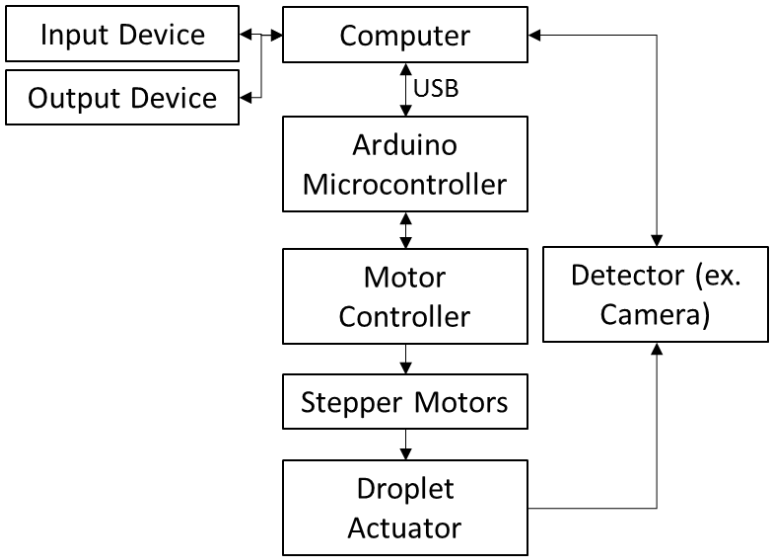

Figure 2.2. Droplet actuation system block diagram.

2.2.2 Superhydrophobic Surface Fabrication

Fabricating the patterned superhydrophobic surface involves two main steps: spray coating the superhydrophobic layer, and ink-jet printing the hydrophilic regions. In this work, letter sized transparency films (Staples Inc.) are used as the substrate for patterning. Each film is cleaned by rinsing with distilled water before the superhydrophobic coating (Rust-Oleum NeverWet) is applied. The coating procedure is a two-step process that requires depositing a base coat and a top coat. The base coat is applied using the supplied aerosol canister by spraying the surface of the transparency film 6-12 inches from the surface as shown in Figure 2.3a. Three applications of the base coat are performed after waiting two minutes between applications. After drying for one hour, the top coat is applied in a similar fashion by spraying the substrate 6-12 inches from the surface with four applications of top coat. The substrate is dried for 12 hours at room temperature before subsequent patterning.

After coating, droplets exhibit contact angles of up to 165°, and droplets roll off the surface when inclined less than 1° from horizontal. Other materials and coatings were also tested, including Teflon AF 1600 and LDPE plastic. The Teflon coating is applied by

spin coating a glass microscope slide (50 mm x 75 mm) with 1% wt/wt Teflon AF 1600 in Fluorinert FC-40 for thirty seconds at 1000 rpm. After spin coating, the coated glass slide is postbaked at 160°C for 10 minutes. The Teflon coating exhibited roll-off angles around 45° from horizontal for 10 μL droplets. The LDPE plastic was tested in two configurations, sanded and non-sanded. The non-sanded LDPE plastic consists of a 0.004 inch thick film (McMaster-Carr). The roll-off angle on this plastic film was similar to Teflon at approximately 45° from horizontal. One group reported that superhydrophobic LDPE surfaces can be formed by lamination onto a wire mesh.[21] The authors concluded that the surface roughness imparted by the wire mesh increases hydrophobicity. To test this effect, our LDPE plastic films were sanded by hand with 240 grit sandpaper. (McMaster Carr). The sanded plastic films demonstrated lower roll-off angles than the non-sanded films, at approximately 10° from horizontal for 10 μL droplets. These alternative surfaces and coating produced higher roll-off angles, indicating lower hydrophobicity than the Neverwet coating. For this reason, Neverwet was chosen as the preferred superhydrophobic coating.

Hydrophilic regions are then patterned on the superhydrophobic substrate by ink-jet printing (Figure 2.3b). The coated transparency film is loaded into the document feeder of an office style ink-jet printer (Epson WF-2540). A standard black ink cartridge (Epson T200120) is used to print the hydrophilic patterns according to a file designed with Adobe Illustrator CC. After printing, the patterned substrate is dried for 12 hours at room temperature to ensure ink stability. The dimensions of the upper platform (10.2 cm by 10.2 cm) allow six devices to be printed on the letter-sized transparency film at a time.

Other methods of patterning the superhydrophobic surface were also tested, including cutting, wax printing, and pen writing. Using an electronic craft cutting machine (Silhouette Cameo, Silhouette America, Inc.), thin lines are cut into the Neverwet surface. This creates a hydrophilic region, as the Neverwet layer no longer covers the transparency film in the cut region. A drawback of this method is that the Neverwet layer is prone to peeling after the cutting process. This peeling effect causes the thin cut lines to become much larger than intended, trapping droplets and prohibiting transport. The wax printing method was also tested with a commercially available wax printer (Xerox ColorQube 8570DN, Xerox). Unlike many dye-based ink-jet printer inks,

wax printing is highly water-resistant, which is a desirable feature. The Neverwet surface is degraded after printing, however, due to the high temperatures and pressures required for wax deposition. The electronic craft cutting machine was fitted with a pen attachment in order to test the pen writing technique with a water resistant pen (Sharpie Ultra Fine). Similar to the ink-jet printing method, hydrophilic regions are created as the pen deposits ink onto the superhydrophobic surface. The two main drawbacks of the pen writing method are clogging and low resolution. After patterning one device, the superhydrophobic surface coating clogs the pen, requiring frequent cleaning. The resolution of pen writing is lower than inkjet printing, as the width of the pen is approximately 1 mm while ink-jet printing is capable of patterning 0.1 mm lines. After testing each of these methods, it was concluded that ink-jet printing produced the highest resolution and longest lasting hydrophilic patterns.

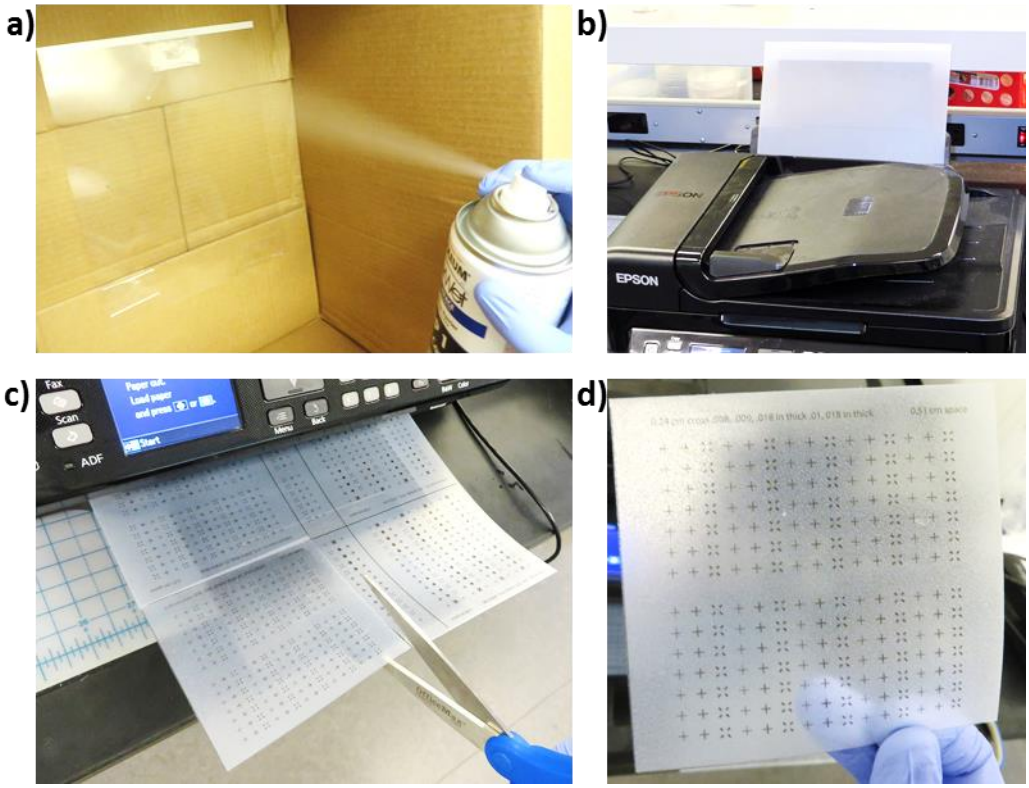

Figure 2.3. Fabrication procedure. **(a)** Apply superhydrophobic coating to the transparency film. **(b)** Print hydrophilic patterns with inkjet printer. **(c)** Cut each device from the patterned transparency film. **(d)** Visually inspect device for defects.

2.3 Results

2.3.1 Transport of Individual Droplets

Droplet transport can be induced using the rapid tilting mechanism. As shown in Figure 2.4, a 10 µL droplet is placed on the cross-shaped symbol. As the upper platform begins tilting to the right, the droplet tends to stay in the initial position. The droplet on the tilted surface adheres to the hydrophilic surface of the cross-shaped symbol. Next, the droplet detaches from the symbol, slides down the inclined substrate, and attaches to a neighboring hydrophilic symbol as the platform returns to a horizontal position. In the droplet actuation system, two actuation forces propel the droplet to roll along the surface: gravitational and rotational force. The adhesion force between the droplet and the hydrophilic symbol oppose these actuation forces. Since the roll-off angle of a 10 µL droplet on the unpatterned superhydrophobic surface is ~0.21 degrees, drag due to this surface is much lower than the hydrophilic adhesion force.

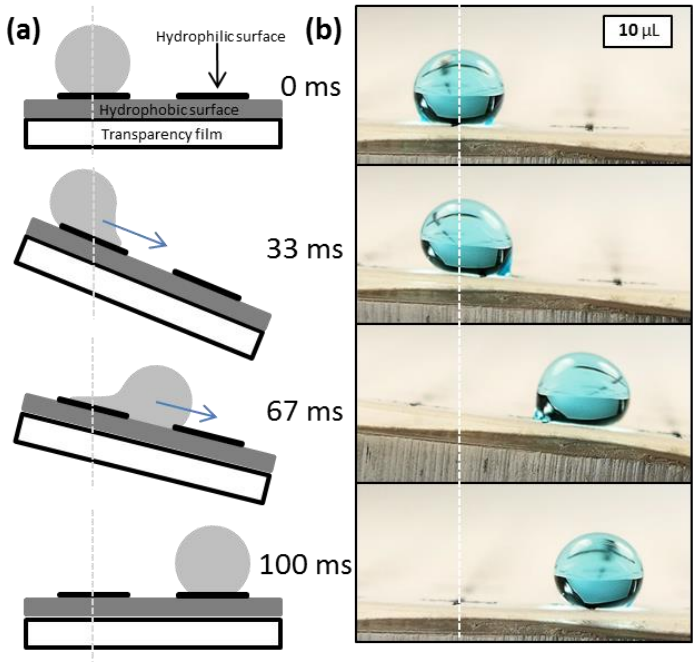

Figure 2.4. Method of droplet transport. **(a)** A droplet is initially positioned on the left hydrophilic design. The substrate is rapidly tilted (110 revolutions per minute) through the stepper motors and their connecting belts. This forces the droplet to move to the right hydrophilic design. The rapid tilting step can be repeated multiple times to move a droplet over a specified distance on the transparency film. **(b)** Image sequence of a single droplet being transported by the abovementioned method.

2.3.2 Adhesion Force

The adhesion forces of three types of cross-shaped symbols were measured by slowly inclining the upper platform until the droplet detached from the symbol. Cross symbols with line thicknesses of 0.006 in., 0.007 in., and 0.008 in. were tested. Droplets of volumes ranging from 20 µL to 40 µL were placed on a cross symbol, then the tilting platform was inclined at a rate of 0.1 degree/second. At the point of detachment, the angle of the platform was recorded, as shown in Table 2.1. Droplet adhesion force was equated to the component of gravitational force acting on the droplet parallel to the surface using the following equation:

$$F = mgsin(\theta) \tag{2.1}$$

Where θ is the detachment angle and m is the droplet mass. Figure 2.5 illustrates the experimental setup and results. As the thickness of the cross symbol increases, the droplet adhesion force increases as well. Droplet volume influences adhesion, as larger droplets cover a larger area of the hydrophilic symbol. From this result, it is clear that modifying the thickness of each hydrophilic symbol allows modulation of the droplet release angle.

Table 2.1. Droplet release angle. As droplet volume increases, the release angle decreases. Symbol line thickness also influences release angle.

	Cross symbol line thickness		
	0.006 in.	0.007 in.	0.008 in.
	Angle (degrees)	Angle (degrees)	Angle (degrees)
20 µL	15.5°	18.6°	-
30 µL	11.0°	14.1°	17.5°
40 µL	9.2°	11.2°	12.9°

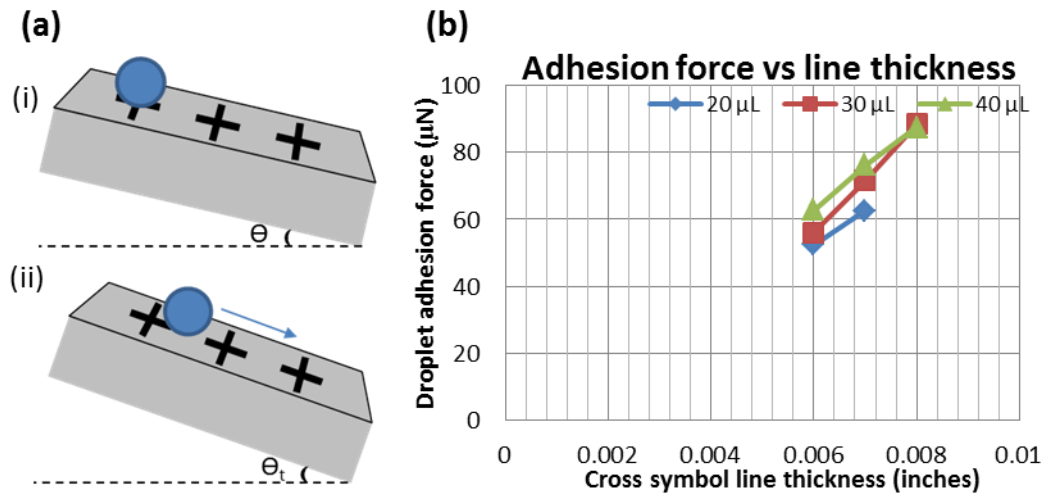

Figure 2.5. Adhesion force vs line thickness. **(a)** Before the threshold angle, the droplet remains on the cross symbol (i), After the threshold angle is reached, the droplet is released from the symbol (ii). **(b)** As the cross thickness increases, the droplet adhesion force increases linearly. The threshold release angles range from 9 degrees to 20 degrees.

2.3.3 Actuation Force

The droplet actuator system relies on two forces to drive droplet movement. As shown above, gravitational force acts upon the droplet, causing droplet release at relatively large angles (~9°-20°). Under normal operation, however, the upper platform is rotated to angles from ~3° to 4.5°. The rapid movement of the platform allows this reduction in tilt angle by providing additional force that acts on the droplet. Figure 2.6 shows the forces that provide droplet actuation as seen from the side view of the platform. The tilt angle (θ) is exaggerated for illustration. The axis of rotation lies 3 cm below the platform (the radius (r) of the circle shown). The distance of the droplet from the center of the platform is shown as distance (d). The radius the droplet travels is given as (R).

Newton's 2nd Law for rotation states:

$$\tau_{net} = I\alpha \qquad (2.2)$$

Where τ_{net} is the net external torque, I is the moment of inertia, and α is the angular acceleration.

When a force is applied perpendicular to the axis of rotation, torque is also given by:

$$\tau_{net} = F \cdot R \qquad (2.3)$$

Where F is the force applied and R is the length of the lever arm

Substituting (2.3) into (2.2):

$$F \cdot R = I\alpha \tag{2.4}$$

The moment of inertia for a point mass is given by:

$$I = mR^2 \tag{2.5}$$

Where m is the mass and R is the perpendicular distance to the rotation axis

Substituting (2.5) into (2.4):

$$F \cdot R = mR^2\alpha \tag{2.6}$$

Angular acceleration is given by:

$$\alpha = \frac{a_t}{R} \tag{2.7}$$

Where a_t is the tangential acceleration and R is the length of the lever arm

Tangential acceleration is given by:

$$a_t = \frac{d|V|}{dt} \tag{2.8}$$

Where V is the velocity of the droplet, and t is time

Droplet velocity is given by:

$$V = 2\pi f R \tag{2.9}$$

Where f is the frequency of rotations per minute (rpm)

Tangential acceleration can be approximated as:

$$a_t \sim \frac{2\pi R \Delta f}{\Delta t} \tag{2.10}$$

Substituting (2.10) into (2.7):

$$\alpha = \frac{2\pi \Delta f}{\Delta t} \tag{2.11}$$

Substituting (2.11) into (2.6) gives the force provided by rapidly tilting the platform. As the platform reaches the maximum tilt angle, Δf changes from ~12 rpm to 0 rpm in $\Delta t \sim$ 0.004 seconds. Δt is determined by the amount of time needed for the platform the stop rotation. This parameter is affected by the tension of the elastomeric rubber tubing. We have found that higher tensions decrease Δt, thereby increasing the force acting on the droplet.

$$F = mR\frac{2\pi \Delta f}{\Delta t} \tag{2.12}$$

The force provided by gravity is given by:

$$F_{g,x} = mg\sin(\theta) \tag{2.13}$$

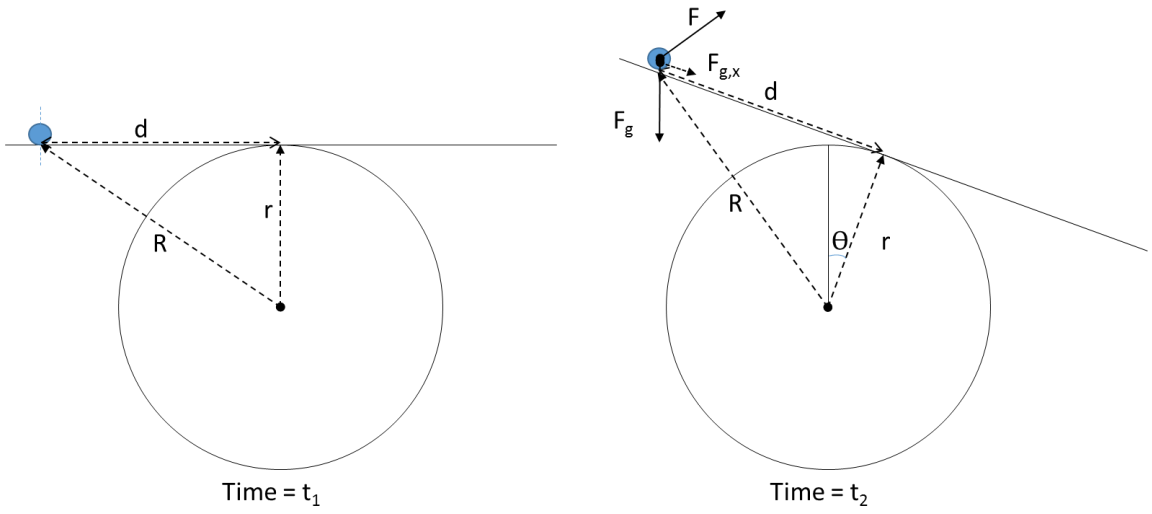

Figure 2.6. Droplet actuation force diagram. The axis of rotation is indicated by the center of the circle, and the horizontal line (time = t_1) represents the surface of the platform. A droplet is placed at a radius R from the axis of rotation. Upon actuation (time = t_2), the droplet experiences gravitational and rotational forces $F_{g,x}$ and F, respectively.

2.3.4 Graphical User Interface

A graphical user interface is written to control the movement of the tilting platform and record the position of each droplet, as shown in Figure 2.7. This allows the user to control the tilting platform intuitively using the keyboard and mouse rather than entering serial commands to each motor. The user interface allows control of motor parameters, such as number of steps and the speed/direction of rotation. By default, the position of the platform is horizontal. By pressing the double arrow buttons, the rotational angle increases in the corresponding direction. The single arrow button rapidly tilts the platform to specified angle, then returns it to the horizontal position. A bubble level (Camco™) is used to ensure that the platform is horizontal before operation. In addition, video preview and video capture options are present.

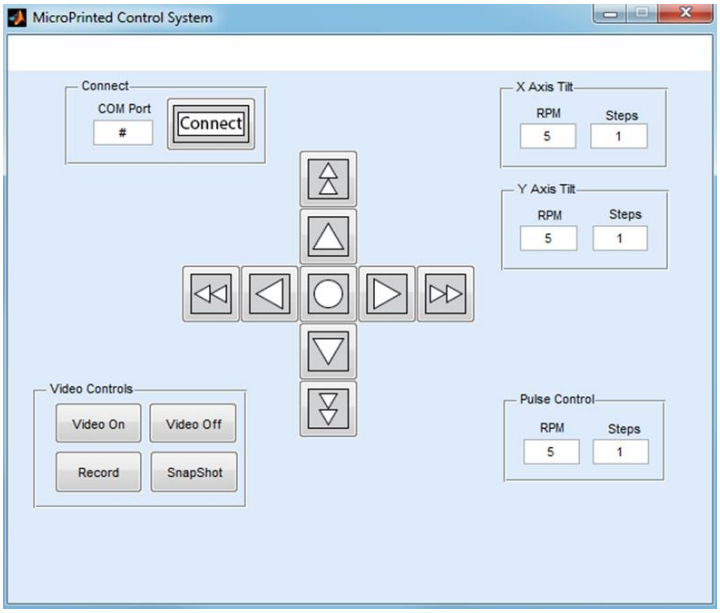

Figure 2.7. Graphical user interface. Single arrow buttons rapidly tilt the platform in the corresponding direction then return to horizontal. Double arrow buttons tilt and hold the platform at a specified angle. The circle button centers the platform horizontally.

2.3.5 Optimization of Transport Symbol

Although slowly inclining the upper platform can allow droplet transport, large threshold angles are needed (9º-20º). After detachment, the droplet is difficult to control as it accelerates down the inclined surface. Using the rapid tilting mechanism, actuation can be achieved at angles between 3º to 5º. Since the platform returns to the horizontal immediately after droplet detachment, the droplet does not accelerate uncontrollably. Droplet transport can be controlled by patterning a series of symbols at a fixed spacing. The optimal symbol patterns for droplet transport were determined by testing several configurations. Two parameters were varied, the cross symbol thickness, and the symbol spacing (center-to-center). The average displacement error of each configuration was measured, shown in Figure 2.8. Negative displacement error denotes failure of the droplet to detach from the cross symbol. For example, if the droplet was expected to move to the adjacent symbol spaced 0.3 cm away, but the droplet failed to move, the error would be -0.3 cm. Conversely, positive error occurs when the droplet travels beyond the adjacent symbol. For each device, the tilting speed and angle of the platform were constant at 2.5 rad/s and 4º, respectively. The droplet volume was 10 µL. As predicted from the adhesion force testing, higher line-thicknesses produced negative displacement error and thinner

lines produced positive error. The optimal line thickness and spacing were 0.008 in. thick at 0.335 cm spacing, which produced an average displacement error of 0.005 cm. This result indicates that the droplet moved sequentially across each cross symbol, with negligible variation in droplet position (1.4%). Consequently, this configuration was used for further testing and development when droplet transport was required. Using rapid tilting, the droplet actuation system can transport droplet volumes as low as 5 µL. The maximum volume that can be transported using one cross symbol is 30 µL. Table 2.2 shows typical actuation parameters for a variety of droplet sizes on different symbol thicknesses.

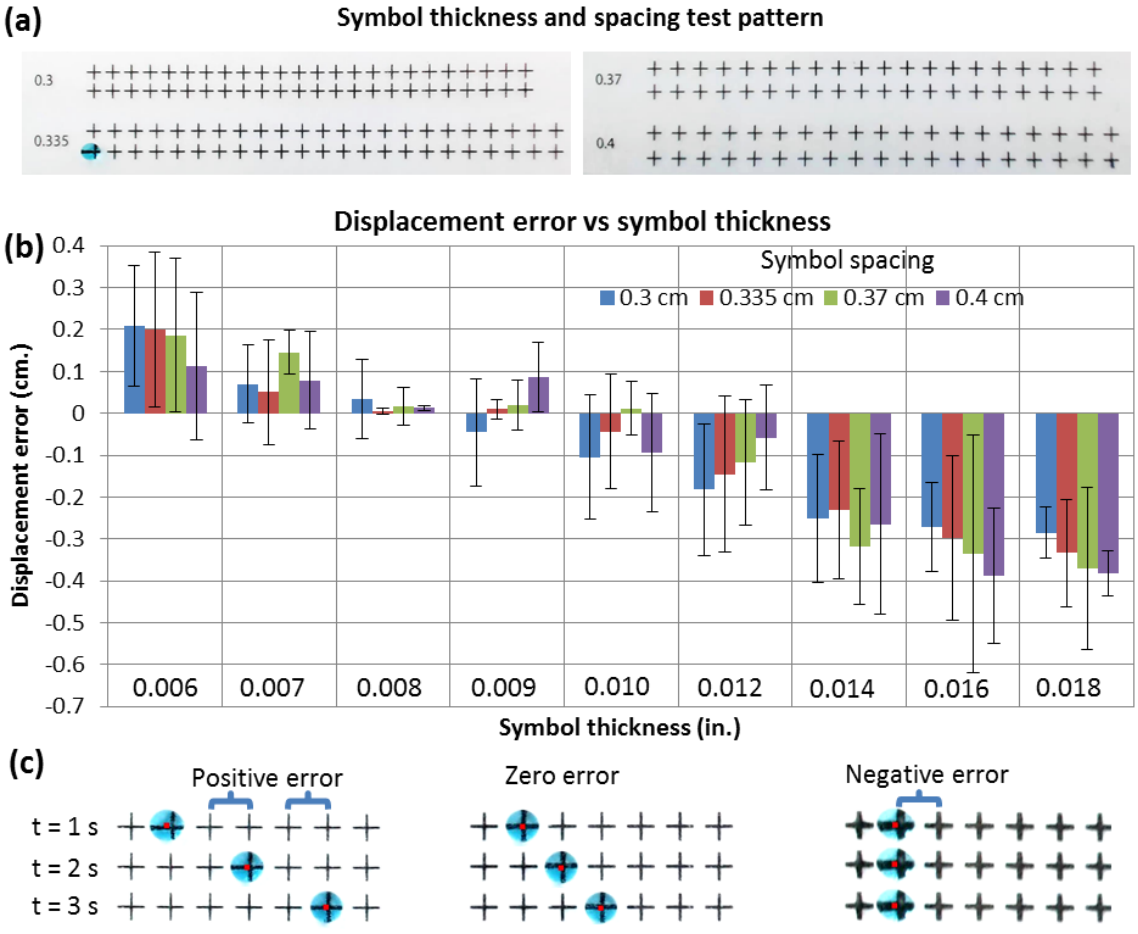

Figure 2.8. Optimization of symbol thickness and spacing. **(a)** Experimental setup: a droplet is placed on a row of cross symbols of varying line thickness and spacing. **(b)** Displacement error for each configuration. **(c)** Illustration of positive error, zero error, and negative error.

Table 2.2. Typical droplet actuation parameters.

Cross symbol line thickness = 0.006 in.				
Droplet volume (µL)	Revolutions per minute		Number of steps	
	Range	Typical	Range	Typical
6	110-130	120	10-15	10 (2.1°)
8	90-130	110	10-16	11 (2.31°)
10	80-120	90	11-17	12 (2.52°)
20	70-120	70	11-15	14 (2.94°)
30	50-110	50	9-18	15 (3.15°)
200*	10-30	20	8-15	11 (2.31°)

Cross symbol line thickness = 0.008 in.				
Droplet volume (µL)	Revolutions per minute		Number of steps	
	Range	Typical	Range	Typical
6	110-130	120	11-16	13 (2.73°)
8	100-130	110	11-16	13 (2.73°)
10	90-130	100	11-17	14 (2.94°)
20	80-120	90	11-17	15 (3.15°)
30	60-110	80	9-18	17 (3.57°)
200*	20-40	30	8-15	13(2.73°)

Cross symbol line thickness = 0.009 in.				
Droplet volume (µL)	Revolution per minute		Number of steps	
	Range	Typical	Range	Typical
6	140-150	150	13-16	15 (3.15°)
8	130-150	150	13-16	15 (3.15°)
10	100-130	110	11-16	15 (3.15°)
20	80-120	90	11-18	16 (3.36°)
30	60-110	80	9-18	17 (3.57°)
200*	30-60	50	9-16	12 (2.52°)

- *Four cross symbols required
- 1 step = 1.8° in motor rotation = 0.21° rotation of upper platform
- Symbol spacing is 0.335 cm
- 1 mL (1000 µL) droplets can be transported using 16 symbols (20 rpm, 10 steps).
- 5 µL droplets can be transported using a single symbol (140 rpm, 11 steps).

2.3.6 Characterization of Dead Volume after Transport

In addition to displacement error, dead volume is an important performance metric for symbol design. A small volume of liquid remains trapped on each symbol after actuation, which comprises the dead volume. In general, larger hydrophilic areas produce larger dead volumes. To measure this parameter, a 10 µL droplet was actuated across 20 cross symbols (0.008 in. line thickness, 0.335 cm spacing). After actuation, the volume of the droplet was measured using a 10 microliter syringe (Hamilton). The volume change of a stationary droplet was measured to control for evaporation. Subtracting the volume change of each droplet gives the dead volume, as shown in Figure 2.9. The average dead volume was 0.14 µL across all twenty symbols, or 7 nL per symbol. This equates to a loss of 0.07% per symbol for a 10 µL droplet.

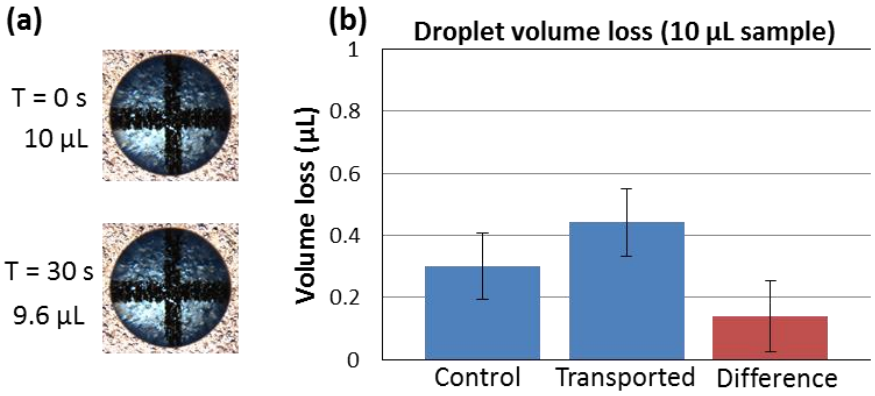

Figure 2.9. Dead volume after transport across 20 symbols. **(a)** After 30 seconds, this droplet (control) lost 0.4 µL due to evaporation. **(b)** The average volume loss of the control droplet (stationary) was 0.3 µL. The transported droplet lost additional volume, indicated by the red bar (0.14 µL).

2.3.7 Transport of Multiple Droplets and Larger Droplets

The droplet actuation system can transport not only single droplets but it can also transport multiple droplets. Using a grid of equally sized cross symbols (0.007 in. line thickness), several droplets placed on the grid can be transported simultaneously (Figure 2.10a). The spacing between two symbols is 0.335 cm. In addition to multiple droplet transport, a large droplet can also be transported on the cross symbol grid. To transport a large droplet (>40 µL), multiple symbols can be used instead of using a single symbol with a large line thickness. If a droplet is positioned on a single thicker symbol, the large hydrophilic surface area strongly attracts the center of the droplet, which increases the dead volume. As shown in Figure 2.10b, an 80 µL droplet is placed on four symbols, and these symbols attach to the corners of the droplet. Reducing the speed and increasing the tilting angle of the stepper motor (80 revolutions per minute, 20 steps) allows transport of the droplet. Using 9 cross-shaped symbols, a 0.3 mL droplet also can be manipulated by applying 20 revolutions per minute with 15 steps, as shown in Figure 2.11.

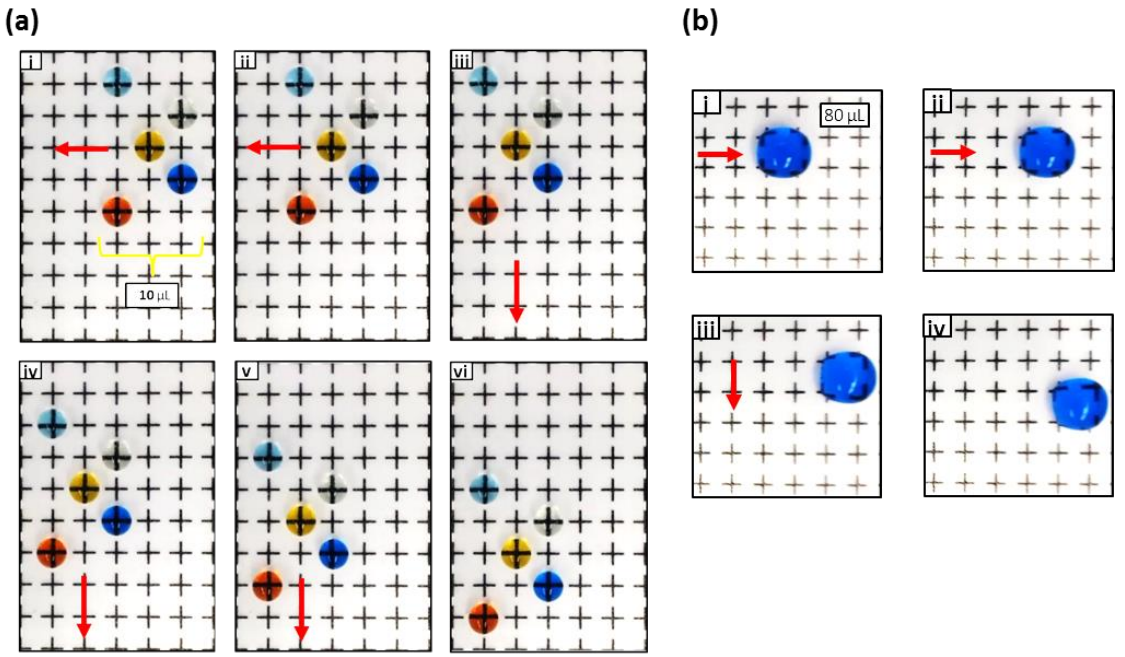

Figure 2.10. **(a)** Transport of multiple liquid droplets: Images sequence illustrates the movement of multiple droplets. The volume of each droplet is 10 µL. Five droplets (shown in different colors) are transported simultaneously. **(b)** Large droplet transport: an 80 µL droplet is transported by decreasing the speed and increasing the tilt angle of the stepper motors (80 revolutions per minutes, 20 steps). Four symbols are combined instead of using one thicker hydrophilic symbol.

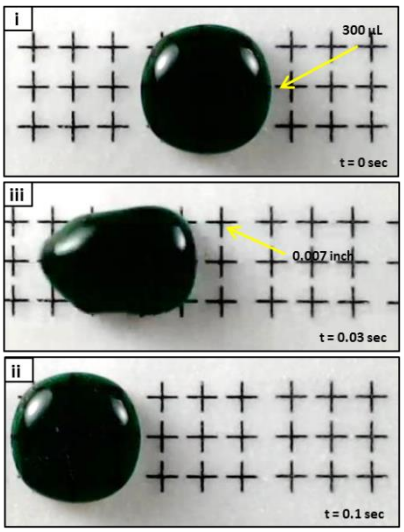

Figure 2.11. Large droplet transport. **(i)** The 300 µL droplet is placed on the nine cross symbol pattern. **(ii, iii)** The droplet is transported to the neighboring symbol.

2.3.8 Merging and Mixing of Droplets

Using symbols with different thicknesses and shapes, the droplet actuator can selectively manipulate droplets in a variety of operations. Cross shaped symbols of different thicknesses can be used to control the merging of two droplets. Merging is one of the most important droplet operations, as nearly every experiment requires this step. It is often necessary to perform a sequence of merging and mixing steps while pausing between each step for a reaction to occur. In Chapter 3, such merging and mixing operations are used to react a glucose sample with a glucose indicator reagent. As shown in Figure 2.12, yellow, red, and blue droplets are placed on cross symbols with line thicknesses of 0.006 in., 0.008 in., and 0.01 in., respectively. As the thicker cross symbols have a larger hydrophilic surface area than the thinner cross symbol, when a user rapidly tilts the upper platform, only the yellow droplet on the thinner symbol is transported. Since a thicker symbol has a greater adhesion force, the droplet on the thicker cross symbol remains stationary. After the yellow and red droplets are merged, rapid mixing is possible by transporting the droplet in a circle or agitating the upper platform with lower speeds and tilt angles to shake the droplet. Finally, the mixed droplet is transported and merged with the blue droplet.

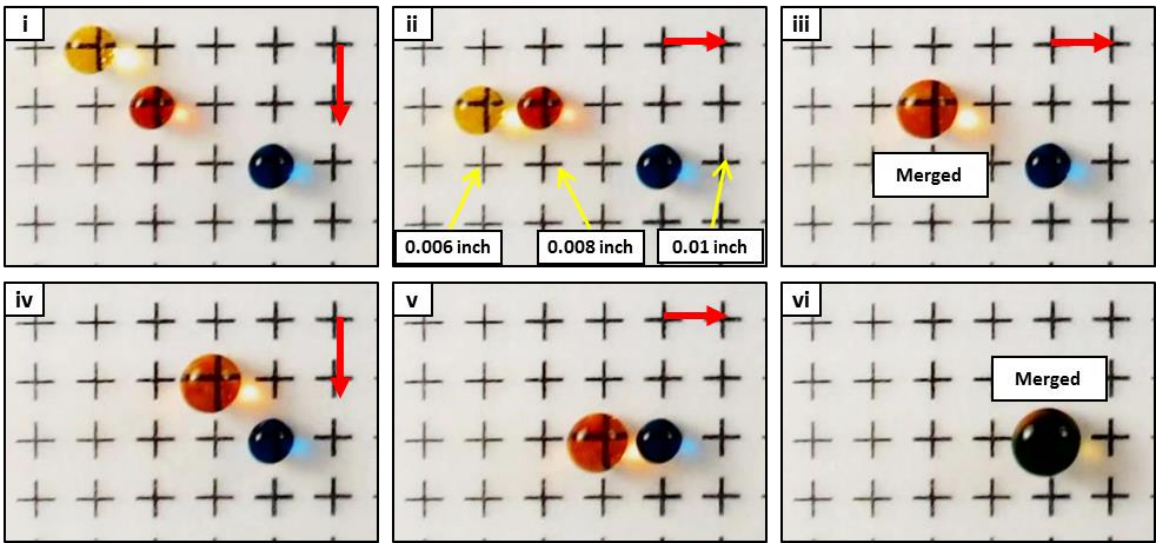

Figure 2.12. Merging droplets. **(i, ii)** The yellow droplet is transported across the 0.006 in. line thickness cross symbols, as the red and blue droplets remain stationary on the thicker cross symbols. **(iii-v)** The yellow and red droplets are merged, then the resulting droplet is transported while the blue droplet remains stationary. **(vi)** The droplets are merged together on the 0.1 in. line thickness cross symbol.

2.3.9 Dispensing Smaller Droplets from a Large Droplet

Droplet dispensing is also possible using a dot symbol, in which a large droplet is split into number of small droplets. Dispensing is often used when an experiment requires a single reagent to be used for multiple reactions. For example, the glucose indicator reagent is reacted with several glucose samples, so dispensing can be performed to reduce the number of manual pipetting steps. Serial dilutions are also possible using the dispensing technique.

As shown in Figure 2.13a, as a 10 µL droplet is transported across the dot symbols, a small amount of liquid is dispensed on each symbol. After dispensing, the red colored droplet is held on a thicker cross shaped symbol and another clear droplet is mixed with the dispensed droplets. As the clear droplet is transported across each dot symbol, the red color intensity increases. Compared to the cross shaped symbol, the total hydrophilic surface area of the dot symbol is smaller. However, the hydrophilic area is concentrated directly under the droplet, which increases the adhesion force. Therefore, as the droplet is transported, a small droplet is dispensed on each symbol. The volume of the droplet dispensed on the symbol is determined by the surface area of the dot.

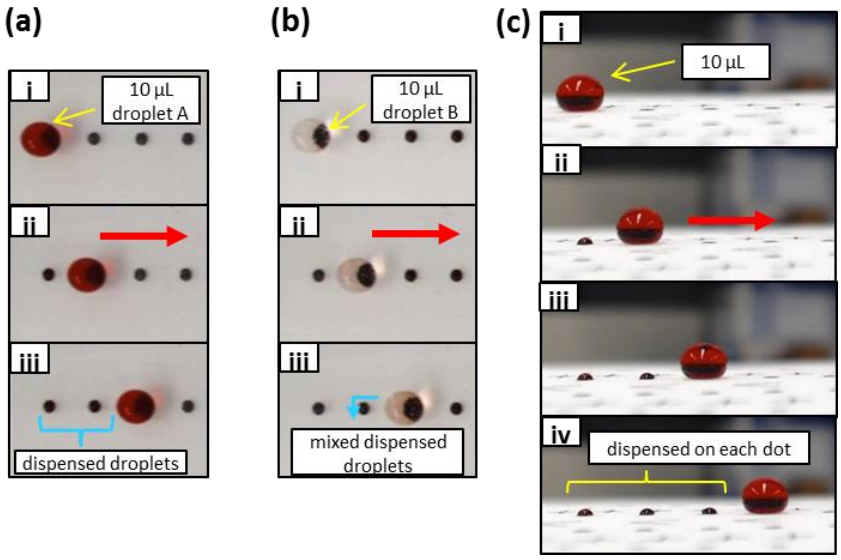

Figure 2.13. Droplet dispensing. **(a)** The red-colored droplet (10 µL) is dispensed on each circular-shaped hydrophilic symbol. As the droplet is transported across these hydrophilic dots, each symbol collects a small volume from the droplet due to adhesion. **(b)** The clear droplet is transported across the dot symbols, causing the red color intensity to increase. **(c)** Side view of the droplet dispensing process.

2.3.10 Directional Droplet Transport

In addition, using a greater-than sign (“>”), the droplet can be restricted from moving in a specific direction. This symbol allows greater flexibility in designing a device capable of sequentially manipulating several droplets. By restricting each droplet to a separate “track,” actuating one droplet would not interfere with the other droplets. Merging is also facilitated by these directional symbols.

As shown in Figure 2.14a, while the droplet on the cross shaped symbol is transported, the droplet on the greater-than sign is not able to move to the left. When the droplet attempts to move to the open side of the greater-than sign, the droplet is stretched as the hydrophilic lines diverge (Figure 2.14a). This increases the adhesion force of the droplet. In the opposite direction, however, the lines converge and meet at a point. This point offers lower adhesion force, which allows the droplet to be transported to the next symbol with a lower speed and tilt angle of the stepper motor (Figure 2.14b). Combining three greater-than signs, a pattern can be made that allows the droplet to move in only one direction (Figure 2.15). Since the closed tips of three greater-than signs are pointing to the center, a droplet only can move to the direction in which no signs are present.

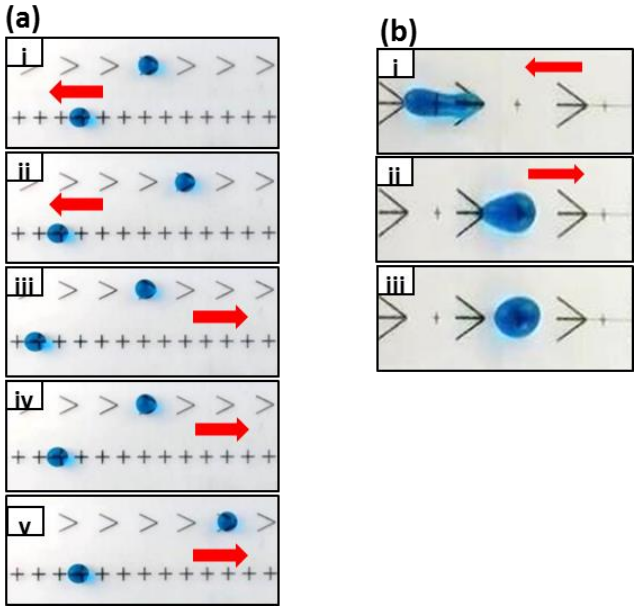

Figure 2.14. Directional droplet transport symbols. **(a)** Droplets on the greater-than symbol are restricted when tilted to the left, where the cross symbol offers no restriction. Both symbols allow droplet transport when tilted to the right. **(b) S**low motion images showing different configurations of the droplet when the upper platform rapidly tilts to the left and right. When tilted to the left, the diagonal lines prevent the droplet from moving to next symbol. The droplet releases when tilted to the right.

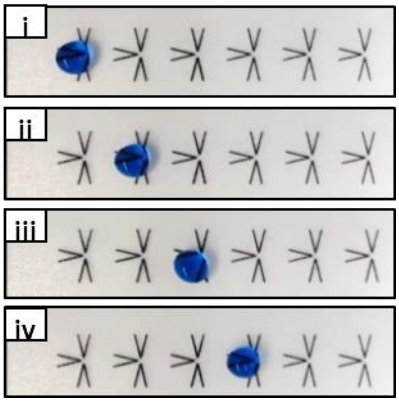

Figure 2.15. One-directional droplet transport symbols. The droplet only moves to the right due to the three greater-than signs pointing the center. One side of the symbol is open, allowing the droplet to be transported to the next symbol.

2.3.11 Magnetic Bead Separation

By placing a permanent magnet beneath the upper platform, droplets containing magnetic beads can be manipulated. Many biological assays rely on magnetic bead separation, including immunoassays for thyroid stimulating hormone and 17β-estradiol as demonstrated on a digital microfluidic system.[22] In this example, magnetic beads are labeled with antibodies that bind with the target analyte, allowing extraction and measurement.

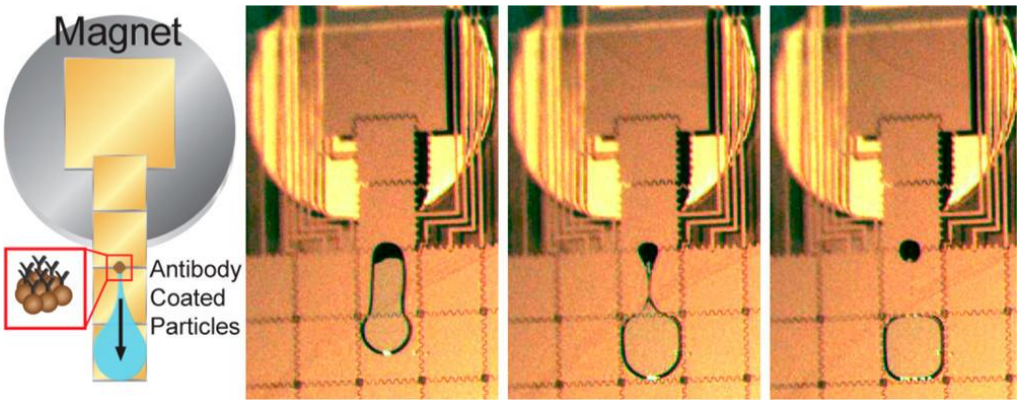

Figure 2.16. Magnetic bead separation for immunoassay on digital microfluidics platform.[22]

Figure 2.17a shows the process of extracting magnetic beads (BioMag superparamagnetic iron oxide, Polysciences, Inc.) from the red droplet. A permanent neodymium magnet (0.5 in. diameter) was placed under the platform, producing a magnetic field strength of 0.4 Tesla. By transporting the droplet, the magnetic particles remain fixed above the magnet while the liquid separates away. The particles can subsequently be resuspended by another blue droplet as shown in Figure 2.17b.

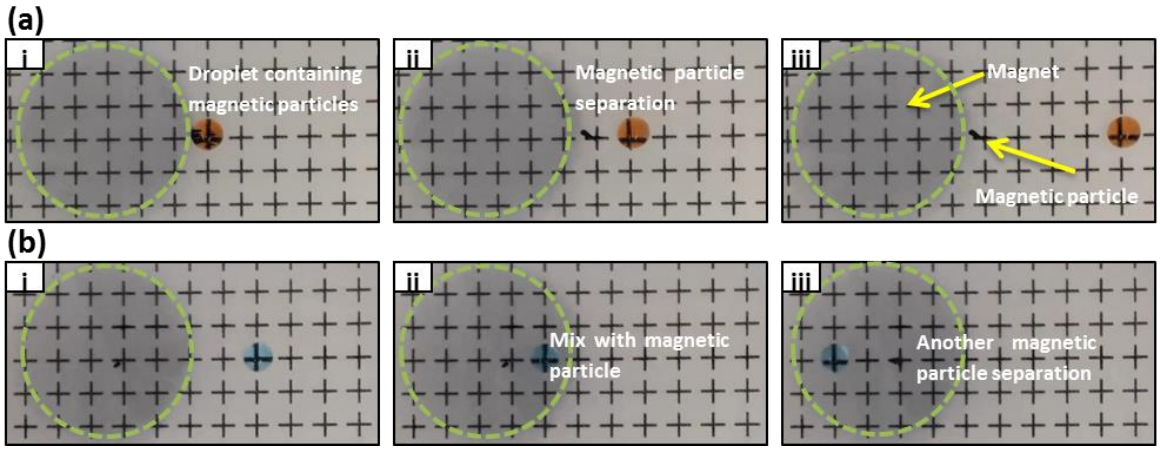

Figure 2.17. Magnetic particle separation. **(a)** Magnetic particles separated from red droplet **(b)** Magnetic particles resuspended by blue droplet.

2.3.12 Closed Surface Operation with Top Plate

Droplet actuation is possible not only using an open surface, but also a superhydrophobic top plate can be used for closed surface operation. As mentioned in Section 2.3.6, droplet volume loss occurs due to evaporation at a rate that depends on temperature and humidity. By applying a top plate, evaporation can be reduced by minimizing the amount of droplet surface area in contact with the air. To fabricate the top plate, a glass microscope slide (50 mm x 75 mm) is coated with NeverWet using the procedure described in Section 2.2.2. Two glass microscope slides (25 mm x 50 mm) are attached to each side of the top plate with double sided tape to act as spacers. These spacers produce a 2 mm gap between the bottom patterned superhydrophobic surface and the top plate. The top plate increases the required tilt speed and angle for actuation compared to the open surface configuration.

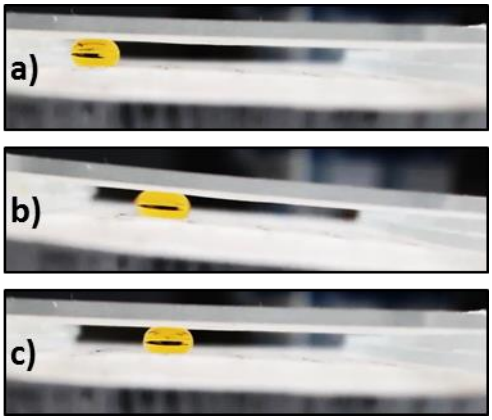

Figure 2.18. Closed surface droplet transport with superhydrophobic top plate.

2.3.13 Dispensing Droplets from a Reservoir

In Section 2.3.9, droplet dispensing was shown using the dot symbol. However, dispensing large droplets with the dot symbol is not possible. To achieve large droplet dispensing, a syringe-based dispenser was developed. In the present design, the syringe is capable of storing 20 mL of liquid, which enables experiments to be repeated without human intervention. Different volumes of liquid can be dispensed, allowing serial dilutions to be performed.

The operation of the dispensing reservoir is shown in Figure 2.19. The 20 mL syringe is stoppered by a 200 µL pipette tip attached to a 1 mL syringe. The tip of the pipette is sealed with cyanoacrylate adhesive along with a steel wire to extend the tip. As the tip of the syringe is facing down, liquid is prevented from flowing by the pipette tip, which acts as a stopper. When the pipette tip is pushed up by depressing the steel wire, liquid is free to flow. The syringe is placed above the upper platform Figure 2.19a, and by rapidly tilting the platform, the steel wire is temporarily depressed and a droplet is dispensed. Multiple droplets can be dispensed either separately or onto the same symbol. The reservoir system allows reagents to be stored without evaporation concerns, as the syringe is sealed by the plunger.

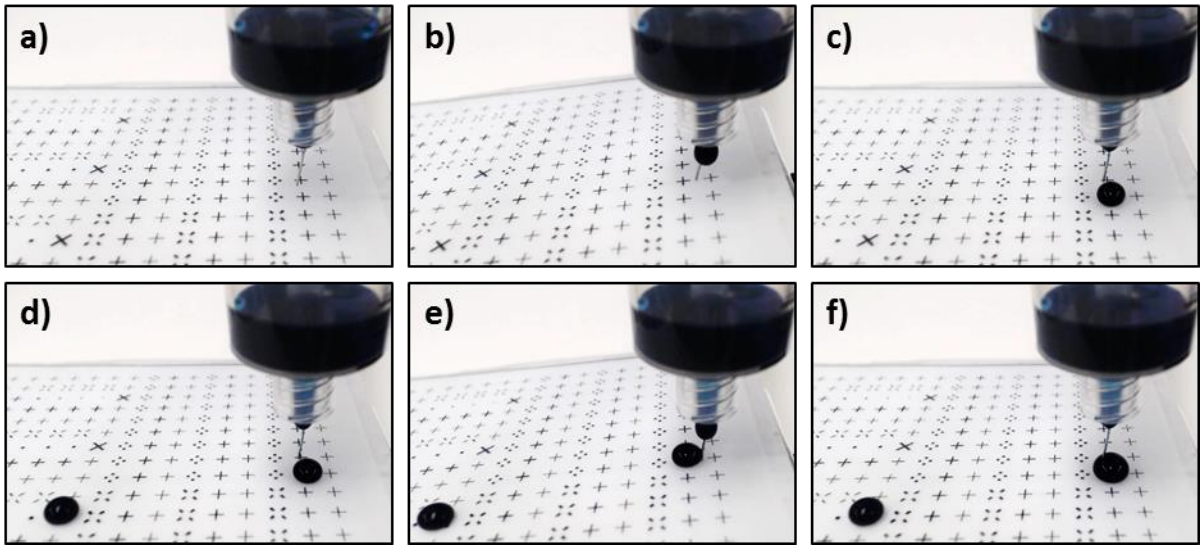

Figure 2.19. Dispensing multiple droplets from large reservoir. **(a)** The dispensing reservoir is places along the edge of the platform. **(b)** The upper platform is tilted such that the dispenser tip is depressed by the surface. **(c)** A droplet is dispensed from the tip, and the upper platform returns to the horizontal position. **(d)** The droplet is transported to another symbol on the surface, and a second droplet is dispensed. **(e,f)** A large droplet can be created by dispensing two droplets in the same location.

2.3.14 Droplet Splitting with a Superhydrophobic Blade

Droplet splitting is another important operation that is possible using the droplet actuator. Splitting can be thought of as symmetrical dispensing, which is often used for serial dilutions or extractions. In digital microfluidic systems, splitting requires activating electrodes on both sides of a droplet, which pulls the droplet in either direction. Configuring the electrode spacing and the gap between the electrode array and top plate are critical to produce the forces necessary to overcome surface tension and achieve splitting.

Figure 2.20 shows the operation of the superhydrophobic blade, which can split droplets of volumes as low as 20 µL. To fabricate the superhydrophobic blade, a NeverWet coating is applied to the edge of a razor blade (X-ACTO) using the procedure described in Section 2.2.2. After coating, the blade is attached to a piece of tape (Nashua Tape 357) which allows the blade to stand vertically. The blade is placed on the patterned superhydrophobic surface, and a droplet is loaded onto the surface facing the blade. Upon rapidly tilting the platform, the droplet collides with the superhydrophobic blade and splits into two separate droplets. Depending on the initial velocity, the droplets can

rebound from the blade or continue past the blade until the droplets adhere to a hydrophilic symbol. After splitting, both droplets can be transported, which offers an advantage over the dot symbol dispensing method, which traps the dispensed droplets.

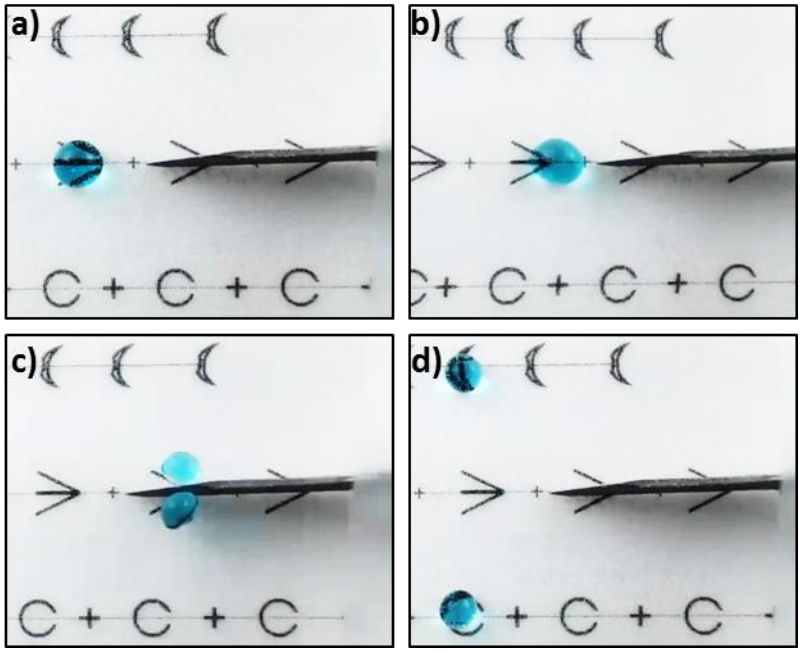

Figure 2.20. Droplet splitting with superhydrophobic blade. **(a)** Initial position **(b)** The upper platform is rapidly tilted to the right **(c)** The droplet is split by the superhydrophobic blade **(d)** The droplets rebound from the blade and adhere to neighboring hydrophilic symbols.

The results shown in Chapter 2 demonstrate the variety of operations that can be performed on the droplet actuator system. Several experiments can be carried out using the transport, mixing, and merging and dispensing steps that are possible using only the patterned superhydrophobic surface. The capabilities of the system can be extended by using additional components such as magnetic particles, top plates, a dispensing reservoirs, and superhydrophobic blades. Components can be added or removed depending on experimental requirements. In Chapter 3, a glucose assay is carried out on the droplet actuator system.

CHAPTER 3
COLORIMETRIC GLUCOSE DETECTION

3.1 Introduction

Glucose concentration is an important parameter for the early diagnosis of diseases related to high sugar levels. Typically, individuals with diabetes have elevated levels of glucose (hyperglycemia) in their bodies that can be detected in blood and other physiological fluids. Without treatment, hyperglycemia leads to diabetic ketoacidosis, which is responsible for over 500,000 hospital days per year at a cost of 2.4 billion USD.[23] Thus, it is increasingly important to monitor glucose levels routinely, especially for people with abovementioned diagnosis.

Currently, glucose meters are often used to measure glucose concentration. Early meters relied on a colorimetric reaction, while current meters use an electrochemical (coulometric method).[24] In both reactions, glucose oxidase is reacted with the sample to generate hydrogen peroxide. Subsequent reactions of the hydrogen peroxide with other reagents can initiate a color change or an electrical current.

Digital microfluidic systems capable of glucose concentration measurement have been demonstrated.[6] The system shown in Figure 3.1 uses an enzyme-based colorimetric assay to determine glucose concentration. As the two droplets are mixed, the reaction produces a darker color. In this example, an LED and photodiode detector were placed on opposite sides of the electrode array so that the amount of light transmitted through the droplet could be measured over time. The photodiode was sensitive to the wavelength of light absorbed by the droplet, which becomes purple over time (540 nm wavelength). Different concentrations of glucose produce differences in reaction rates that can be measured using the system. A calibration curve can be made using glucose standards of known concentration.

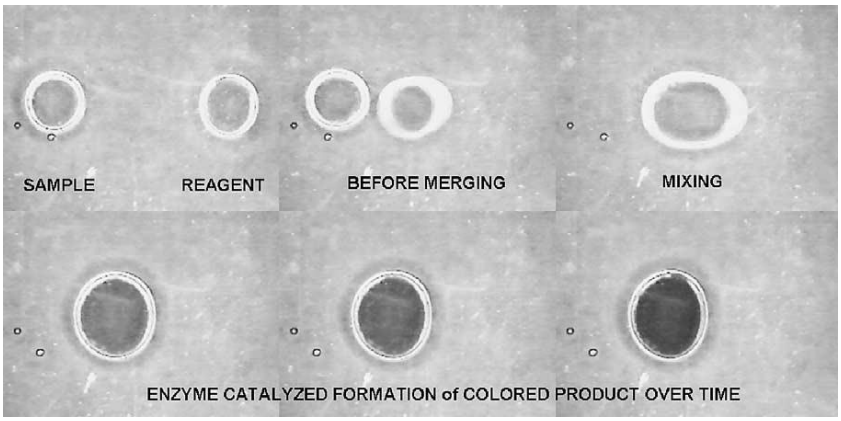

Figure 3.1. Glucose assay on digital microfluidic system.[6]

A similar glucose detection assay was developed using our rotational droplet actuator. Instead of an LED and photodiode to measure light absorbance, a camera (Logitech C920) was used to detect changes in color intensity over time. Using this method, multiple reactions were monitored at once on the same device. The accuracy of the camera-based measurement was compared to a laboratory microplate reader (BioTek ELx808). The glucose concentrations of two sheep serum samples were measured using both methods.

3.2 Experimental

3.2.1 Chemicals

The glucose reagent is composed of the following chemicals: glucose oxidase (Sigma-Aldrich, G6125), peroxidase (Sigma-Aldrich, P8125), TOPS (N-ethly-N-sulfopropyl-m-toluidine) (Sigma-Aldrich, E8506), and 4-aminoantipyrin (Sigma-Aldrich, A4382). Glucose standard (Sigma-Aldrich, G6918) was also used. The glucose reagent was prepared with 3 U/mL glucose oxidase, 3 U/mL peroxidase, 5 mM TOPS in 0.1 M phosphate buffered saline (pH 7.0), and 3 mM 4-aminoantipyrine. The glucose standard solution was diluted to create 1 mg/mL, 0.75 mg/mL, 0.5 mg/mL, 0.25 mg/mL, and 0.1 mg/mL standards in deionized water. For the microplate reader experiment, glucose (HK) assay reagent (Sigma-Aldrich, GAHK20) was prepared by resuspending the vial contents with deionized water. The glucose (HK) reagent contains 1.5 mM NAD, 1.0 unit/ml of glucose-6-phosphate dehydrogenase with sodium benzoate and potassium sorbate as preservatives.

3.2.2 Glucose Measurement on Microplate Reader

A microplate reader (BioTek ELx808) was used to create a standard curve and to measure the glucose concentration of two sheep serum samples. A 96 well plate is used to contain each reaction. Three replicates of each glucose standard (concentrations between 0.1 and 0.75 mg/mL) are used to create the standard curve. In addition, three replicates of each sheep serum (Sigma-Aldrich, S3772) and blank samples are loaded into the well plate. 20 µL of sample is loaded into each well, then 180 µL of glucose (HK) reagent is added. The well plate is immediately loaded into the microplate reader. UV absorbance measurements are taken at 340 nm wavelength every minute.

The results of the absorbance change over time for each sample is shown in Figure 3.3. To determine the standard curve, the "max v" measurement was taken from the microplate reader software (Gen5 Data Analysis Software, BioTek). This measurement corresponds to the maximum rate of change in absorbance during the period between 5 and 15 minutes after the reaction was initiated. As shown in Figure 3.3b, the standard curve is linear for the concentrations used in the experiment. By interpolating the best fit line, the glucose concentrations of the sheep serum samples were calculated to be 0.63 mg/mL and 0.65 mg/mL. These samples were purchased from Sigma-Aldrich in two separate bottles, so small variations in glucose concentration are reasonable.

3.2.3 Glucose Detection Assay on Droplet Actuator

The droplet actuator can also be used for real-time monitoring of glucose concentration using a colorimetric enzyme-kinetic method. A glucose indicator reagent solution was prepared by mixing glucose oxidase, peroxidase, 4-amino antipyrine (4-AAP) and N-ethyl-Nsulfopropyl-m-toluidine (TOPS) in the concentrations mentioned in Section 3.2.1. This glucose reagent differs from the previous reagent in that the color change occurs in the visible spectrum (545 nm wavelength) rather than ultraviolet (340 nm wavelength) for the glucose (HK) reagent. This reaction occurs in two steps. First, the glucose oxidase oxidizes the glucose to produce hydrogen peroxide and gluconic acid. Then, the 4-amino antipyrine and TOPS reacts with the hydrogen peroxide to produce

quinoneimine, which absorbs 545 nm light. The chemical reaction sequence is shown below:

$$glucose + H_2O + O_2 \xrightarrow{glucose\ oxidase} gluconic\ acid + H_2O_2$$

$$2H_2O_2 + 4 - AAP + TOPS \xrightarrow{peroxidase} quinoneimine + 4H_2O$$

Figure 3.2 illustrates the configuration of the patterned device used to perform the glucose assay. Glucose standard droplets (concentrations between 0.1 mg/mL and 0.5 mg/mL) are placed on the first column of the patterned device and the reagent droplets are positioned on the second column of the patterned device. The glucose standard droplets then merge into the reagent droplets. The mixture of the two droplets is transported to third column. The symbols in the third column are designed with an open area in the center to provide a white background for determining the color intensity of the droplets. The top substrate is tilted in each direction at low speeds to mix the chemicals thoroughly. After the reaction is completed, the color intensity of each droplet over time is extracted from the recorded video using a Matlab script.

The results of the experiment are shown in Figure 3.3c-d. The video from the camera is converted to grayscale, and average pixel value is sampled from the center region of each droplet every 10 seconds. These values are normalized by computing the $\log_{10}$ ratio of the initial pixel value of the droplet over the current pixel value at each time point. As the reaction occurs, the current pixel value becomes lower (darker) and the $\log_{10}$ ratio increases. The increase is proportional to the glucose concentration, which allows a standard curve to be calculated using a similar method to the microplate reader. Figure 3.3d shows the standard curve, which was created by calculating the maximum change in $\log_{10}$ ratio after the first minute of the reaction for each droplet. To stay within the linear range, the serum sample was diluted in deionized water by a factor of 2. By interpolating the best fit line, the serum glucose concentration was calculated to be 0.32 mg/mL. After correcting for 2X dilution factor, the concentration is 0.64 mg/mL, which closely matches the result from the microplate reader (0.63 mg/mL).

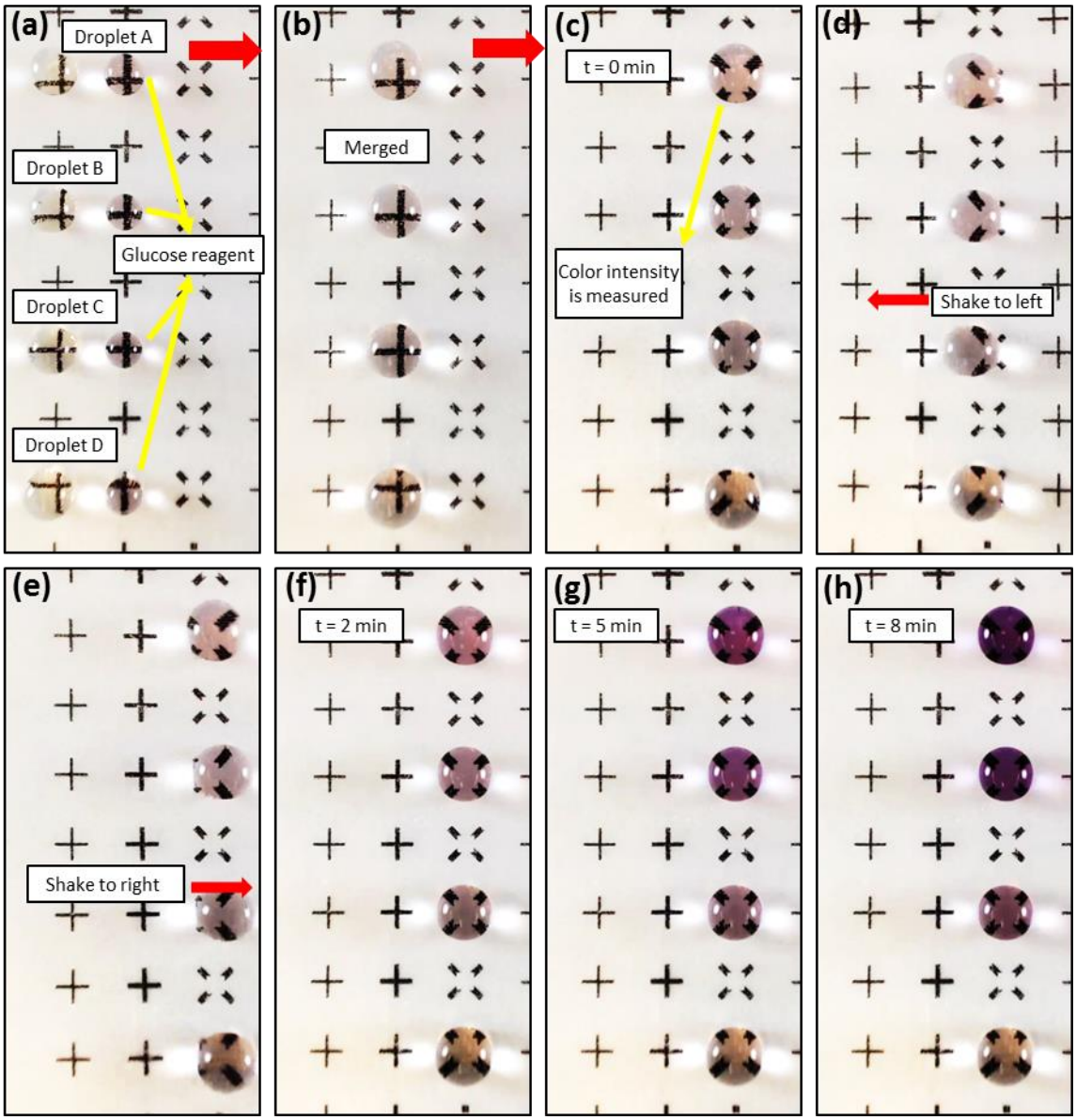

Figure 3.2. Glucose standard testing: **(a)** glucose standards of different concentrations are placed on the platform. **(b)** Next, the glucose reagent is simultaneously mixed with each glucose standard. **(c)** The color intensity of each droplet is measured over an eight minute time period. **(d,e)** The droplets are gently shaken to the right and left to enhance mixing. **(f-h)** Color intensity increases as the reaction continues.

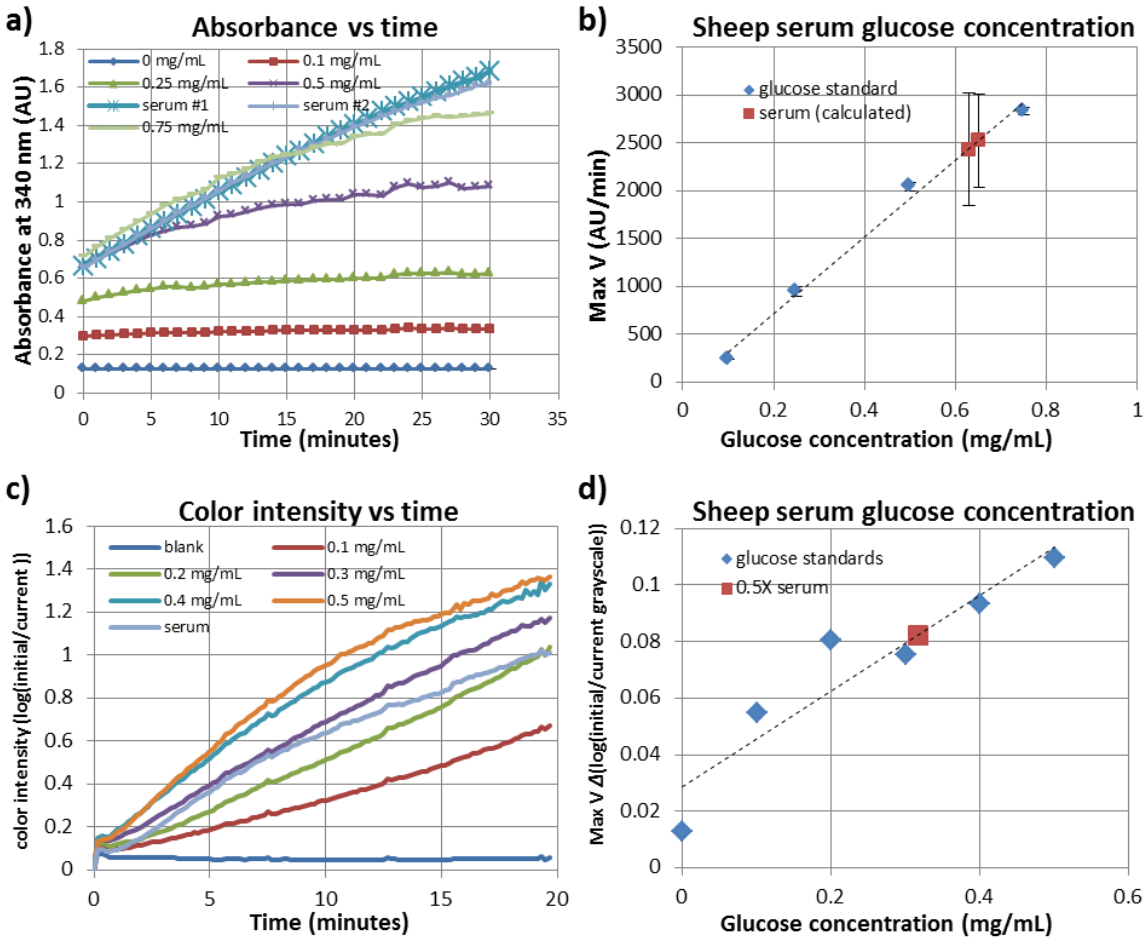

Figure 3.3. Comparison of glucose concentration measurements obtained with a microplate reader **(a,b)** and with the camera **(c,d)**.

3.2.4 Sensitivity and Detection Limit

The sensitivity of the camera based color detection is determined by the characteristics of the enzymatic reaction. According to Michaelis-Menten kinetics[6,25], the rate equation is given by:

$$V(t) = \frac{k_r E_0 S(t)}{S(t)+K_M} \tag{3.1}$$

$$V_i = V_{max}\frac{[glucose]}{K_M \times DF} \; if \; \frac{[glucose]}{DF} \ll K_M \tag{3.2}$$

Where [glucose] represents the glucose concentration, DF is the dilution factor of the sample, and K_M is the Michaelis constant, V_i is the initial reaction rate, and V_{max} is the maximum reaction rate. The sensitivity is limited by the maximum rate of reaction

(V_{max}), the extinction coefficient of quinoneimine (ε), the path length (L), and the dilution factor (DF) as shown by the following equation[6]:

$$S = \frac{\varepsilon L V_{max}}{K_M \times DF} \quad (3.3)$$

This equation represents the slope of the standard curve, which was 0.1698 AU mL/min mg.

The detection limit of the system is related to the sensitivity of the reaction as well as the bits of information in each pixel. Since the camera produces an 8-bit greyscale image, and approximately 15 points are required to establish an accurate linear fit, the minimum change in color intensity that can be detected by the camera is 15 units over the course of the experiment. The $\log_{10}$ ratio for this minimum change is $log_{10}\left(\frac{2^8}{2^8-15}\right) = 0.0263$. For the current experiment, the maximum rate of color change occurs within the first 5 minutes. The detection limit in this case is given by the following equation:

$$C_{min} = \frac{0.0263}{5S} \quad (3.4)$$

Where S is the sensitivity of the reaction. The detection limit of the system is therefore 0.031 mg/mL.

3.2.5 Dispensing Glucose Reagent

In order to more easily and accurately dispense the glucose reagent, a new patterned device was created, as shown in Figure 3.4. Instead of loading a separate glucose reagent droplet onto each symbol, a single droplet is used. First, the glucose reagent is transported across the dot symbols Figure 3.4a-d before being trapped on the thick x-shaped symbol. Each dot symbol retains a portion of the droplet, as discussed in Section 2.3.9. After dispensing, the four sample droplets are merged with the glucose reagent, then transported to the open cross symbol for color measurement.

This patterned device showcases the capabilities of the droplet actuator system. Each droplet operation is used, including dispensing, single and multi-droplet transport, merging, and mixing. The design allows parallel analysis of many droplets and reduces the number of pipetting steps required to perform the experiment. Scaling up the experiment is also simple, as twelve or more of these four-sample patterns can be operated at once.

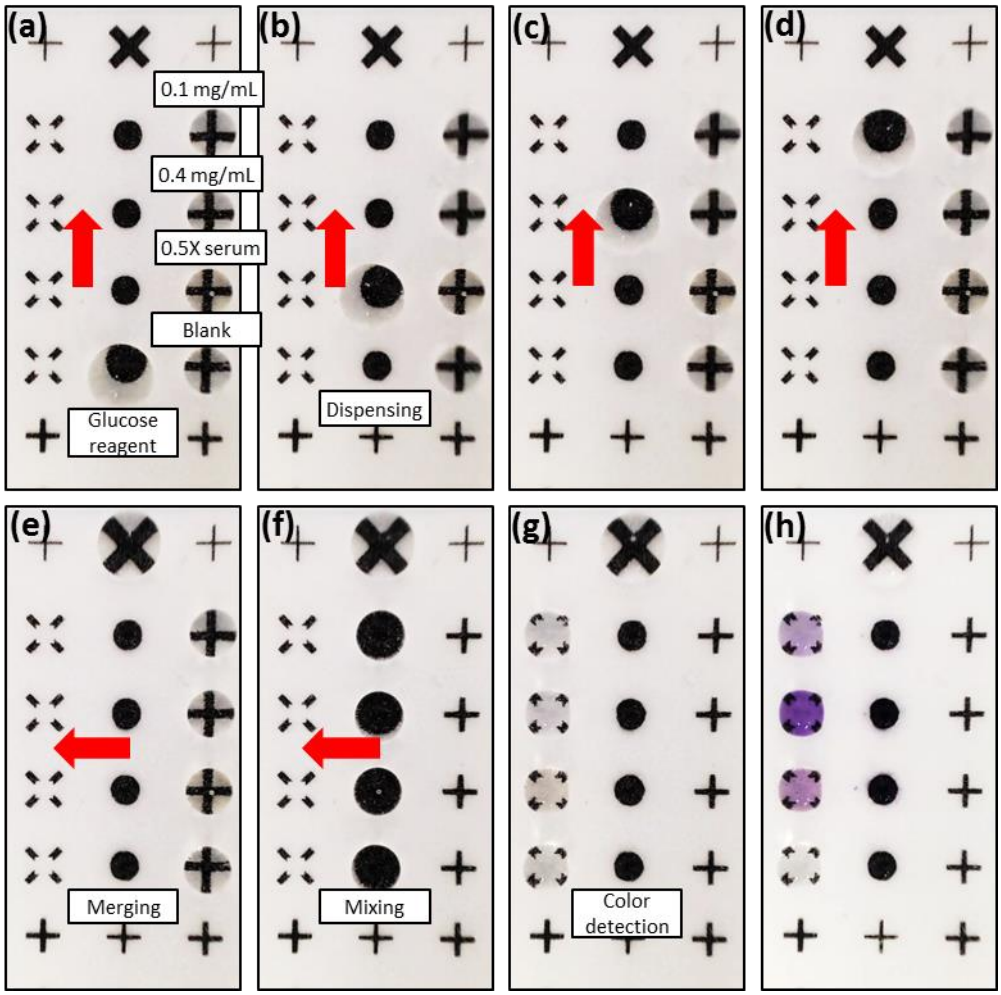

Figure 3.4. Dispensing glucose reagent. **(a-d)** Glucose reagent dispensed on each dot symbol. **(e)** Glucose standards and sheep serum merged with reagent. **(f)** Merged droplets are mixed by gentle shaking **(g,h)** Color intensity is measured for 15 minutes.

These results demonstrate the capabilities of the droplet actuator system in performing biological assays. Colorimetric assays are used to detect proteins, acids, and HIV, among others.[26-28] Using the same droplet operations, these assays could be adapted to work on the droplet actuator as well. The automated dispensing, mixing and colorimetric testing offers many possibilities that can be performed on the device that costs ~$200 USD and utilizes a simple fabrication process.

3.3 Provisional Patent

This work is part of a provisional patent (Application number 62153121) filed on Apr. 27, 2015.

REFERENCES

1. Klingenberg, M. "When a common problem meets an ingenious mind," *EMBO Reports*, *6*(9), 797–800. (2005).

2. Pollack, M. G., Fair, R. B., & Shenderov, A.D., "Electrowetting-based actuation of liquid droplets for microfluidic applications," *Applied Physics Letters*, *77*(11), 1725. (2000).

3. Chang Y. H., Lee G.B., Huang F. C., Chen Y. Y., Lin J. L., "Integrated polymerase chain reaction chips utilizing digital microfluidics," *Biomedical Microdevices* 8:215–25. (2006).

4. Barbulovic-Nad I., Au S. H., Wheeler A. R., "A microfluidic platform for complete mammalian cell culture," *Lab on a Chip*, 10:1536–42. (2010).

5. Rastogi V., Velev O. D., "Development and evaluation of realistic microbioassays in freely suspended droplets on a chip," *Biomicrofluidics* 1:014107. (2007).

6. Srinivasan V., Pamula V. K., Fair R. B., "Droplet-based microfluidic lab-on-a-chip for glucose detection," *Analytica Chimica Acta*, 507:145–50. (2004).

7. Jebrail M. J., Bartsch M. S., Patel K. D., "Digital microfluidics: a versatile tool for applications in chemistry, biology and medicine," *Lab on a Chip*, 12, 2452–2463. (2012).

8. Sista R.S., Eckhardt A. E., Wang T., Graham C., Rouse J. L., Norton, S. M., Srinivasan, V., Pollack, M. G., Tolun, A. A., Bali, D., Millington, D. S., Pamula, V. K., "Digital microfluidic platform for multiplexing enzyme assays: implications for lysosomal storage disease screening in newborns," *Clinical Chemistry*. 57:1444–51. (2011).

9. Brassard, D., Malic, L., Normandin, F., Tabrizian, M., Veres, T., "Water-oil core-shell droplets for electrowetting-based digital microfluidic devices," *Lab on a Chip*, *8*(8), 1342–1349. (2008).

10. Choi, K., Ng, A. H. C., Fobel, R., Wheeler, A. R., "Digital Microfluidics," *Annual Review of Analytical Chemistry*, *5*(1), 413–440. (2012).

11. Mousa, N. A, Jebrail, M. J., Yang, H., Abdelgawad, M., Metalnikov, P., Chen, J., Wheeler, A.R., Casper, R. F., "Droplet-scale estrogen assays in breast tissue, blood, and serum," *Science Translational Medicine*, *1*(1), 1ra2. (2009)

12. Hong L., Pan, T., "Surface microfluidics fabricated by photopatternable superhydrophobic nanocomposite," *Microfluidics and Nanofluidics*, 10, 991–997. (2011).

13. Chiou, P. Y., Moon, H., Toshiyoshi, H., Kim, C. J., & Wu, M. C., "Light actuation of liquid by optoelectrowetting," *Sensors and Actuators, A: Physical*, *104*(3), 222–228. (2003).

14. Guttenberg, Z., Muller, H., Habermüller, H., Geisbauer, A., Pipper, J., Felbel J., Kielpinski, M., Scriba, J., Wixforth, A., "Planar chip device for PCR and hybridization with surface acoustic wave pump," *Lab on a Chip*, *5*(3), 308–317. (2005).

15. Rida, A., Fernandez, V., Gijs, M. A. M., "Long-range transport of magnetic microbeads using simple planar coils placed in a uniform magnetostatic field," *Applied Physics Letters*, *83*(12), 2396–2398. (2003).

16. Ohashi, T., Kuyama, H., Hanafusa, N., Togawa, Y., "A simple device using magnetic transportation for droplet-based PCR," *Biomedical Microdevices*, *9*(5), 695–702. (2007).

17. Duncombe, T. A., Erdem, E. Y., Shastry, A., Baskaran, R., Böhringer, K. F., "Controlling liquid drops with texture ratchets," *Advanced Materials*, *24*(12), 1545–1550. (2012).

18. Lam, P., Wynne, K. J., Wnek, G. E., "Surface-Tension-Confined Microfluidics," *Langmuir*, 18, 948–951. (2002).

19. Ghosh, A., Ganguly, R., Schutzius, T. M., Megaridis, C. M., "Wettability patterning for high-rate, pumpless fluid transport on open, non-planar microfluidic platforms," *Lab on a Chip*, *14*(9), 1538–50. (2014).

20. Elsharkawy, M., Schutzius, T. M., Megaridis, C. M., "Inkjet patterned superhydrophobic paper for open-air surface microfluidic devices," *Lab on a Chip*, *14*(6), 1168–75. (2014).

21. Xu, Q. F., Mondal, B., Lyons, A. M., "Fabricating superhydrophobic polymer surfaces with excellent abrasion resistance by a simple lamination templating method," *ACS Applied Materials and Interfaces*, 3(9), 3508–3514. (2011).

22. Ng, A. H. C., Choi, K., Luoma, R. P., Robinson, J. M., Wheeler, A. R., "Digital microfluidic magnetic separation for particle-based immunoassays," *Analytical Chemistry*, *84*(20), 8805–8812. (2012).

23. Kitabchi, A. E., Umpierrez, G. E., Miles, J. M., & Fisher, J. N., "Hyperglycemic crises in adult patients with diabetes," *Diabetes Care*, *32*(7), 1335–1343. (2009).

24. Clarke, S. F., Foster, J. R., "A history of blood glucose meters and their role in self-monitoring of diabetes mellitus," *British Journal of Biomedical Science*, *69*(2), 83–93. (2012).

25. Chen, W., Niepel, M., Sorger, P., "Classic and contemporary approaches to modeling biochemical reactions," *Genes & Development*, 1861–1875. (2010).

26. Wang, W., Wu, W. Y., Wang, W., Zhu, J. J., "Tree-shaped paper strip for semiquantitative colorimetric detection of protein with self-calibration," *Journal of Chromatography A*, *1217*(24), 3896–3899. (2010).

27. Dungchai, W., Chailapakul, O., Henry, C. S., "Use of multiple colorimetric indicators for paper-based microfluidic devices." *Analytica Chimica Acta*, *674*(2), 227–233. (2010).

28. Shen, L., Hagen, J. a., Papautsky, I., "Point-of-care colorimetric detection with a smartphone," *Lab on a Chip*, *12*(21), 4240. (2012).